**TITLE**

# The BRCA1- RAD51 Axis Regulates SCAI/REV3 Dependent Replication Fork Maintenance

**AUTHOR LIST**

Chloe Unterseher[1, #], Hiroshi Tsuchida[1, #], Rosevalentine Bosire[1], Shaylee Kieffer[1], Xuhui Jin[1] and Richard O. Adeyemi[1,2*]

**AFFILIATIONS**

[1]Basic Sciences Division, Fred Hutchinson Cancer Center, Seattle, WA 98109
[2]Department of Biochemistry, University of Washington, Seattle WA 98195

# These authors contributed equally.

* Corresponding author:
Richard Adeyemi, D.V.M., Ph.D.,
Basic Sciences Division, Fred Hutchinson Cancer Center,
1100 Fairview Ave, Mail Stop A1-162, Seattle, WA 98109, U.S.A.
Phone (office): (206)667-6263
Email: radeyemi@fredhutch.org

ABSTRACT

Replication stress is a key contributor to genomic instability and cancers. BRCA1 has well established roles in protecting stalled forks against degradation. Here we show that BRCA1 has a fork protection-independent role via regulation of RAD51 in a manner that confers dependency on SCAI and REV3. SCAI loss leads to elevated DNA breaks, genomic instability and cell death upon DNA damage. We show that the increased DNA breaks occur in S phase, consistent with fork breakage. BRCA1 drives SLX4-SLX1-ERCC1 mediated DNA break formation in the absence of SCAI and REV3, which are required to maintain integrity of stalled forks for efficient restart. Domain analysis revealed that the increased break signaling seen in the absence of SCAI does not require binding to resection factors like CtIP. Surprisingly, loss of fork reversal factors leads to additive increases in damage signaling and elevated fork shortening in the absence of SCAI/REV3 in a manner that depends on RAD51 activity. We propose that Protexin may be required to replicate through and maintain stalled replication forks at fragile genomic regions. Failure to do so leads to increased DNA breakage and genomic instability.

Keywords: DNA repair, replication stress, homologous recombination, BRCA1, RAD51, REV3, SCAI, SMARCAL1, SLX4, fork reversal, fork maintenance, fork collapse

## INTRODUCTION

Faithful duplication of the genome of dividing cells is continually threatened by impediments that challenge replication fork progression[1]. Such obstacles can result from lesions arising from exogenous DNA damage or from endogenous sources such as DNA secondary structures, difficult-to-replicate chromatin, oncogene-driven hyper-replication, and transcription-replication conflicts, among others[2]. Collectively, these inputs result in replication stress and, if left unresolved, drive fork stalling, breakage, and collapse with subsequent genome instability—a key hallmark of several cancers[3,4]. To avert these outcomes, cells deploy a coordinated replication-stress response that stabilizes perturbed forks, remodels fork architecture, and re-establishes DNA synthesis through pathway choices that include repriming, translesion synthesis (TLS), template switching, and recombination-based restart[5].

A central remodeling route at stalled forks is fork reversal—conversion of the stalled fork into a four-way duplex intermediate—catalyzed by annealing helicases/ATP-dependent translocases such as SMARCAL1, ZRANB3, and others[6,7]. Fork reversal can protect against further damage, yet reversed forks are intrinsically vulnerable. Homologous recombination (HR) factors, most notably RAD51 and BRCA1/BRCA2, extend their canonical roles beyond two-ended double strand break (DSB) repair to stabilize and protect nascent strands at reversed forks[8,9]. However, the varied functions of these proteins at stalled forks and how these differ from conventional two-ended breaks is still not clear.

In addition, how stalled forks transition back to productive replication remains an area of active investigation[10,11]. In addition to RAD51's fork protective function, several studies have shown that RAD51 drives reversal of stalled forks and is important for promoting fork restart [12,13]. Forks can restart via repriming[14] (which suppresses fork reversal and leaves post-replicative single-stranded DNA gaps to be filled later by template switching or TLS) or via direct RECQ1 activity on reversed forks[15]. Alternatively, stalled or reversed forks can be cleaved by structure-specific endonucleases (e.g., MUS81–EME1, SLX1–SLX4), generating one-ended DSBs that are repaired via recombination-based restart[16,17]. In mammalian cells, such restart often resembles break-induced replication (BIR)—a conservative, long-tract synthesis program that, in several contexts, operates with minimal contribution from RAD51's strand-exchange activity [18,19]. Alternatively, RAD51 dependent recombination restart mechanisms without break formation have also been proposed[20,21].

We previously identified a general requirement for the Protexin complex—comprising SCAI and the Pol ζ catalytic subunit REV3—in promoting viability after replicative damage[22]. In particular, we uncovered a TLS-independent function of SCAI/REV3 in the response to DNA interstrand crosslinks (ICLs), where SCAI restrains excessive EXO1-mediated resection and preserves replication competence. These findings, however, raised the possibility that SCAI/REV3 does more than modulate a single nuclease axis at ICLs but may influence other aspects stalled-fork metabolism. Here, we investigate how the SCAI/REV3 complex regulates fork advancement and how the complex

interfaces with the RAD51/BRCA1 module to govern outcomes at stalled forks. We show that SCAI/REV3 is required to maintain fork integrity during replication stress and to promote efficient fork restart. In the absence of SCAI, there is increased replication stress associated DNA breakage in S phase, genomic instability and cell death. Strikingly, break formation in the absence of Protexin is orchestrated by BRCA1-RAD51 via recruitment of SLX4 to chromatin. Furthermore, combined loss of SMARCAL1 and SCAI led to additive break-induced damage signaling and defective fork maintenance. We propose that Protexin loss causes a failure of strand invasion mediated fork restart with resultant fork breakage and genomic instability.

## RESULTS

### Protexin complex prevents DNA breakage and genomic instability following replication stress

We and others previously identified SCAI as a key factor in interstrand crosslink repair[22,23]. Our previous work also suggested that SCAI might prevent cell death upon replication stress. Indeed, consistent with previous findings in U2OS cells, colony formation assays in RPE1 cells showed that SCAI depletion led to diminished viability upon treatment with hydroxyurea (HU) (Figure S1A & B). To examine how loss of SCAI impacted damage signaling following replication fork stalling, RPE1 cells were transfected with two different siRNAs to SCAI, treated with HU and blotted for replication stress markers. As expected, and consistent with what was observed following treatment with crosslinking agents[22], SCAI loss led to increases in CHK1 and RPA2 phosphorylation (Figure 1A). Upon SCAI depletion with either siRNA, we also observed significantly increased phosphorylation of H2AX (hereafter γH2AX), typically a marker of elevated replication stress and/or DSBs, without any changes to H2AX protein amounts (Figure 1A). To further examine this, we made use of U2OS cells engineered to knock out SCAI using CRISPR. In this cell type, we observed similar increases in γH2AX and RPA2 phosphorylated on S4/8 (hereafter pRPA) (Figure 1B). Upon HU treatment, the increased pRPA in ΔSCAI cells could be rescued by re-introducing SCAI (Figure 1C, compare lanes 2, 4 & 6). To further explore SCAI's function during replication stress, we treated cells with aphidicolin, a DNA polymerase alpha inhibitor that also causes replication stress and fork stalling[24,25]. Similar to what was observed following HU treatment, SCAI depletion led to increased γH2AX and pRPA upon treatment with aphidicolin (Figure 1D), showing that this altered signaling stemmed from a dependency on SCAI at distressed forks.

To examine whether REV3 shared similar roles with SCAI in preventing DNA damage at distressed forks, we depleted REV3 using siRNAs. Similar to what was observed upon SCAI loss, REV3 depletion led to increases in pRPA and γH2AX upon fork stalling (Figure 1E, compare lanes 2 and 4). As an orthogonal approach, we examined replication stress signaling events using immunofluorescence (IF) microscopy. To determine whether the observed increased pRPA signified increases on chromatin, cells were pre-extracted to remove unbound proteins. Depletion of either SCAI or REV3 led to increased intensity of RPA upon HU treatment, suggesting that increased pRPA occurred on chromatin (Figure S1C). We also observed increased γH2AX using this approach (Figure S1D).

130 REV3 has well characterized roles in translesion synthesis[26,27]. Because HU is
131 not thought to lead to formation of DNA adducts[28], increased damage signaling upon
132 REV3 loss might be independent of REV3's role in performing TLS across damaged
133 DNA bases. To further examine this, we depleted cells of REV7, which is critical for TLS
134 as a component of DNA polymerase zeta[29]. Whereas REV3 loss led to increases in
135 pRPA and γH2AX after HU treatment, REV7 depletion (and thus inhibition of TLS) did
136 not (Figure 1E, compare lanes 4 and 6). To directly test whether failure of TLS would
137 result in increased damage signaling we treated cells with a previously reported TLS
138 inhibitor[30]. Similar to REV7 depletion, TLS inhibition did not increase pRPA and γH2AX
139 after replication stress (Figure S1E) suggesting that stalled fork induced damage
140 signaling upon REV3 loss was not attributable to a TLS function of REV3. Depletion of
141 REV3 in SCAI knockout (KO) cells did not significantly alter the amounts of pRPA and
142 γH2AX suggesting that both proteins function in the same pathway (Figure S1F).
143 The above data show that SCAI is required to prevent cell death after replication
144 stress. The heightened signaling markers are suggestive of DNA breakage. To
145 investigate whether SCAI loss leads to increased breaks and genomic stability after
146 replication stress, we first treated cells with HU as before, then released from HU
147 treatment and allowed cells to proceed into mitosis (Figure 1F, top panel). We then
148 performed mitotic DNA spreads to examine for the presence of chromosomal
149 abnormalities including breaks, gaps, fusions and similar events. SCAI loss did not
150 significantly impact the extent of chromosomal abnormalities observed in the absence of
151 HU treatment. In contrast, following treatment with HU, we observed that loss of SCAI
152 led to significant increases in the amount of broken and otherwise abnormal chromatids
153 compared to control knockdown cells (Figure 1F & G). The elevated abnormalities
154 prompted us to directly examine whether SCAI limited DNA break formation. To test this,
155 we performed neutral comet assays under a similar timeline but without releasing from
156 HU. This should prevent mitotic entry and allow us to determine whether SCAI loss led
157 to DNA breaks prior to mitosis. Depletion of SCAI led to significant increases in DNA
158 break formation following replication stress compared to controls in both RPE1 (Figure
159 1H) and U2OS cells (Figure 1I). Similar results were seen with REV3 depletion (shown
160 later in Figure 4E). Taken together, these data show that the Protexin complex is
161 required for efficient repair and viability following replication stress and that its loss
162 results in elevated DNA breakage and heightened genomic instability.
163
164 **SCAI/REV3 prevent DNA breakage in S phase**
165 Having shown that SCAI loss upon replication stress led to increased damage
166 signaling with increased DNA breakage, we next sought to understand the kinetics and
167 determine when the DNA breaks form. We hypothesized that the breaks resulted from
168 distressed forks and thus occurred in S phase. We first performed IF assays using well
169 established fixation protocols that allow detection of PCNA specifically in S phase[31].
170 These experiments were done over a time course (Figure S2A-C). We co-stained for
171 γH2AX and, as expected, observed increased γH2AX in SCAI KD cells by 16 following
172 treatment with HU compared to controls (Figure S2A-C). There was high concordance
173 between cells in S phase and cells exhibiting γH2AX staining (Figure S2D-E). At 8 h
174 following HU treatment, only around 25% of cells on average were PCNA-positive,
175 however, when comparing the observed frequency of PCNA/γH2AX double-positive

176 cells to the expected overlap based on independent staining frequencies, we detected a
177 significant enrichment of co-staining that was more pronounced upon SCAI depletion
178 (Figure 2A & B). These findings indicate that the increased DNA damage signaling
179 observed upon HU treatment in SCAI KD cells occurs predominantly in S-phase.
180 Performing similar experiments by immunoblotting, pChk1 was rapidly seen 4h after HU
181 treatment (Figure S2F). pRPA and γH2AX did not however appear until later (Figure
182 S2F). Because western blotting examines the entire population of cells, many of which
183 are outside of S phase, we synchronized cells at the G1/S boundary using double
184 thymidine block and performed a similar time course. Under these conditions, loss of
185 SCAI rapidly led to significant increases in γH2AX by 4 - 8h after HU treatment (Figure
186 2C). Parallel cell cycle analyses revealed that these cells were largely in S phase at this
187 time (Figure S2G) and would remain so due to HU-induced S phase arrest[32].
188 To directly determine whether the increased signaling occurred in S phase
189 populations, we performed flow cytometry experiments where we coupled cell cycle
190 analysis using DAPI with staining for γH2AX and pRPA over a 16-hour time course. This
191 analysis showed a negligible population of cells with increased γH2AX at baseline.
192 These mostly had near 4N DNA content indicating that these cells were either in G2 or
193 M phase. By 8h following treatment with HU however, we observed rapid increase in
194 cells exhibiting phosphorylated H2AX in both WT and SCAI knockdown cells (Figure
195 2D). Based on their DNA content, these increased population appeared to be of cells in
196 S phase. Over the course of treatment, while the absolute numbers of cells exhibiting
197 γH2AX staining were not significantly different at early time points, by 12 after treatment
198 onwards, SCAI knockdown cells exhibited significant increases in the population of cells
199 showing γH2AX staining (Figure 2D-E). Importantly, a population of cells exhibiting
200 abnormally high levels of γH2AX was further increased upon loss of SCAI (Figure 2D-
201 E). pRPA S4/8 is sometimes used as a marker for DNA breakage levels[33,34] and,
202 examining pRPA, both by western and flow cytometry, we observed similar changes in
203 pRPA that mirrored γH2AX accumulation (Figure 2C-2E).
204 To further understand how DNA damage signaling was impacting cells in S phase
205 upon SCAI or REV3 loss, we performed quantitative image-based cytometry (QIBC)[34].
206 This was done following pre-extraction of unbound proteins to examine chromatin
207 bound RPA and γH2AX. We found that loss of either SCAI or REV3 led to increased
208 amounts of chromatin associated RPA (Figure 2F-H) and, consistent with the IF data,
209 increased population of γH2AX that was occurring in cells with S phase DNA content
210 (Figure 2F-H). Compared to flow cytometry, QIBC affords the added advantage of
211 visually comparing intensities of signaling on a per cell basis. Loss of either SCAI or
212 REV3 led to increased intensity of γH2AX and chromatin associated RPA by 16 h after
213 HU treatment (Figure 2G-H). To determine whether the increased γH2AX staining was
214 occurring in the proximity of active replication forks, we performed proximity ligation
215 assays (PLA) using antibodies against PCNA and γH2AX. For this assay we employed
216 our optimized a protocol wherein PCNA is only detected in S phase. In the absence of
217 HU, we failed to observe substantial association between PCNA and γH2AX (Figure
218 S2H-I). Upon HU treatment however, we observed strong increases in PLA signals
219 indicating close association between PCNA (and thus replication forks) and γH2AX
220 staining (Figure S2H-I). PLA did not show differences between SCAI and control KD
221 cells despite increased γH2AX staining seen by several other approaches (Figure 2).

222 This was not surprising since HU generally causes moderate γH2AX (see Figure 2D)
223 and PLA includes an amplification step that could minimize differences. Taken together,
224 these experiments in which we observed increased chromatin bound total and pRPA as
225 well as increased γH2AX in S phase cells upon Protexin loss, are suggestive of
226 increased fork breakage. To directly examine whether SCAI loss induced increases in
227 S-phase DNA breakage, we performed neutral comet assays following a similar cell
228 synchronization protocol as above (Figure S2G). We found that loss of SCAI led to
229 increases in DNA breakage 24 h after HU treatment (Figure S2J), when the vast
230 majority of cells where still in S phase. Taken together, using a combination of
231 approaches, we demonstrate that Protexin loss leads to increased DNA breakage in S
232 phase.
233
234 **Protexin complex is required to maintain fork integrity during replication stress**
235 Our observed increases in S phase DNA damage and break formation suggests
236 a dependency on Protexin to maintain fork integrity. To directly investigate SCAI's role in
237 replication fork dynamics, we performed DNA fiber analysis. We pretreated cells with the
238 first label, added HU for similar duration as our previous experiments, then released
239 from HU while changing labels for a short duration (Figure 3A, top). This setup allows us
240 to measure different potential effects of SCAI loss following replication stress. Under this
241 setup, SCAI loss led to reduced lengths of both the first and second labels suggesting
242 that SCAI was required for maintaining fork integrity upon replication stress (Figure 3B).
243 Knockdown of REV3 also led to a similar phenotype (Figure S3A). Reduced length of
244 the second label suggested that SCAI influenced the efficiency of fork restart. Thus, we
245 quantified the percentage of restarted (dual labeled) forks. We observed modest
246 reduction in the frequency of restart events upon SCAI loss (Figure 3C). SCAI's role
247 appeared to be limited to ongoing distressed forks, as SCAI depletion did not affect the
248 lengths (Figure S3B, left panel) or frequency (Figure S3B, right panel) of new origin
249 firing events (fibers incorporating only the second label) after HU release. Our
250 observation that SCAI/REV3 loss caused reduced lengths of the first label under
251 prolonged replication stress (Figure 1A, left panel) suggested that fork advancement
252 during or following conditions of replication stress was compromised by loss of Protexin.
253 To further understand SCAI's role under these conditions, we switched our labeling
254 strategy to introduce the second label along with HU treatment. SCAI loss consistently
255 led to reduced fork lengths upon replicative stress induction (Figure 3D, right panel) with
256 no significant effect on the first label preceding HU treatment and fork stalling (Figure
257 3D, left panel). Taken together, these data show that SCAI is required to maintain
258 stalled fork integrity under and to promote efficient restart following prolonged
259 replication stress.
260 It is known that absolute blocks to fork advancement can lead to fork reversal
261 with subsequent fork degradation[7,35,36]. We and others have previously reported that
262 SCAI regulates EXO1 activity[22,37]. To examine this further, we co-depleted EXO1 and
263 SCAI and performed similar fork dynamics assays as in Figure 3D. As expected, SCAI
264 loss led to reduced fork lengths upon replication stress (Figure 3E, right panel) without
265 affecting lengths under untreated conditions (Figure 3E, left panel). Surprisingly, co-
266 depletion of EXO1 had no effect on fork lengths in the absence of SCAI under these
267 conditions (Figure 3E), suggesting that the fork defects could not be fully explained by

268 EXO1-mediated fork degradation. Perhaps consistent with this finding, EXO1 depletion
269 failed to rescue HU treatment-mediated increases in pRPA seen upon SCAI loss (Figure
270 S3C). Overall, these results demonstrate that Protexin was required for efficient fork
271 advancement upon and following replication stress. This function of SCAI appeared to
272 not be strongly impacted by loss of EXO1.
273
274 **BRCA1 promotes S-phase DNA break formation in the absence of Protexin**
275 BRCA1 has multiple roles in regulating stalled fork dynamics[38,39]. Thus, we
276 investigated whether BRCA1 might influence the increases in pRPA and γH2AX
277 observed in the SCAI knockdown cells. To test this, we made use of RPE1 cell lines in
278 which BRCA1 had been eliminated using CRISPR and examined for alteration in pRPA
279 and γH2AX levels. As expected, SCAI depletion led to increased damage signaling
280 upon HU treatment (Figure 4A, compare lanes 2 & 3) in BRCA1 proficient RPE1 cells.
281 Strikingly, loss of BRCA1 abolished the increased γH2AX and pRPA seen upon SCAI
282 loss (Figure 4A, compare lanes 3 & 5). As an alternative approach, we depleted BRCA1
283 using siRNA. Consistent with our KO data, the increased pRPA and γH2AX seen upon
284 SCAI loss was eliminated by BRCA1 depletion (Figure S4A). BARD1 is a key interaction
285 partner that forms a stable complex with BRCA1[40]. We depleted cells of BARD1 and, as
286 expected, observed diminished levels of BRCA1 (Figure S4A). Basal levels of pRPA
287 and γH2AX were higher in BARD1 knockdown vs BRCA1 knockdown cells for unclear
288 reasons, nevertheless, BARD1 knockdown dampened increases in pRPA and γH2AX
289 upon SCAI loss (Figure S4A). Depletion of either BRCA1 or BARD1 also eliminated
290 increased pRPA upon cisplatin treatment (Figure S4B). It is worth noting that BRCA1
291 loss did not cause similar reductions in pCHK1 activation (Figure 4B and Figure S4B)
292 suggesting that ATR activity *per se* (which regulates damage signaling upon replication
293 stress) was not affected by loss of BRCA1.
294 To see if a similar effect applied to REV3, we depleted SCAI and REV3 using
295 siRNAs in WT or BRCA1 KO cells. As shown earlier, we observed increases in damage
296 signaling markers indicative of DNA breakage and resection upon loss of either SCAI or
297 REV3 (Figure 4B, compare lane 3 with lanes 5 & 7). Importantly, cell lines lacking
298 BRCA1 failed to show such increases (Figure 4B, compare 5 & 6 and lanes 7 & 8),
299 suggesting that BRCA1 mediates heightened damage signaling in the absence of the
300 Protexin complex. These findings were further confirmed using IF experiments, where
301 loss of BRCA1 led to reduced amounts of RPA on chromatin as well as decreased
302 γH2AX levels, again demonstrating a key role for BRCA1 in mediating damage
303 signaling upon Protexin loss (Figure 4C-D). We showed earlier that SCAI loss leads to
304 elevated DNA breakage (Figure 1J-K). To directly examine if BRCA1 regulates DNA
305 breakage after SCAI/REV3 depletion, we performed neutral comet assays. As expected,
306 loss of either SCAI or REV3 led to increased accumulation of DNA breaks (Figure 4E).
307 Importantly, co-depletion of BRCA1 alongside SCAI prevented DNA break accumulation
308 (Figure 4E), suggesting that the DNA breakage seen in the absence of SCAI was
309 dependent on BRCA1 activity.
310 SCAI binds to ssDNA[23]. We were curious whether BRCA1 loss influenced SCAI's
311 recruitment to damaged chromatin. We treated WT or BRCA1 deficient cells with HU
312 and performed chromatin fractionation experiments. As expected, absence of SCAI
313 caused increased γH2AX (Figure S4C, compare lanes 2 & 3), that was BRCA1

314 dependent (Figure S4C, compare lanes 3 & 5). Importantly, SCAI accumulated in
315 chromatin fractions upon HU treatment (Figure S4C, compare lanes 1 and 2) but this
316 increase in SCAI accumulation was not impacted by BRCA1 loss (Figure S4C, compare
317 lanes 2 & 4).
318 Finally, to directly examine whether BRCA1 orchestrated DNA breakage in S
319 phase, we performed flow cytometry experiments. We tracked DNA content using DAPI
320 and stained for pRPA and γH2AX. As shown earlier, in WT cells, SCAI depletion led to
321 increases in both pRPA and γH2AX in S-phase populations (Figure 4F-H). Strikingly,
322 this increase was abolished upon BRCA1 depletion (Figure 4F-H). Comet assays
323 performed on synchronized S phase populations also showed DNA breaks induced
324 upon SCAI loss was abolished following BRCA1 depletion (Figure S4D). Importantly,
325 the BRCA1 effect was not due to cell cycle dysregulation, as BRCA1 loss by itself did
326 not prevent entry into S phase (Figure S4E) except for minor increases in G2
327 populations as has been reported previously[41,42]. Taken together, our results
328 demonstrate that BRCA1 promotes DNA breakage in the absence of Protexin following
329 induction of replication stress.
330
331 **Defining BRCA1 requirements for regulating stalled fork breakage**
332 BRCA1 forms several complexes important for resection control, HR and other
333 roles; these different complexes often mediate the various functions of BRCA1[43,44]. For
334 example, the BRCA1-CtIP complex, formed via CtIP binding to the C-terminus of
335 BRCA1, controls resection at ionizing radiation-induced DSBs[45,46]. Since BRCA1
336 controls DNA breakage upon SCAI loss, we wanted to determine which subcomplexes
337 and/or function of BRCA1 mediated this role. We first depleted ABRA1, BRIP1 or CtIP
338 (key members of the BRCA1-A, B or C complexes) respectively. Unlike BRCA1
339 depletion, depletion of none of these factors prevented increased pRPA in the absence
340 of SCAI (Figure 5A). We did however observe that depletion of Abraxas by itself
341 increased the basal level of pRPA under HU treatment conditions (Figure 5A, lane 4).
342 Such a role for ABRA1 (Abraxas) has been reported following treatment with the
343 topoisomerase inhibitor, camptothecin[47]. Similar results were seen upon cisplatin
344 treatment (Figure 5B).
345 Next, we examined domain requirements of BRCA1 for DNA breakage upon
346 SCAI loss using previously reported BRCA1 mutant-expressing cell lines[48]. Increased
347 BRCA1 dependent damage signaling upon loss of either SCAI or REV3 could be almost
348 fully rescued by reintroducing tagged WT-BRCA1 into knockout cell lines (Figure S5A-
349 B). We then examined the role of two domain mutants of BRCA1. First, a point mutation
350 (S1655A) in the BRCT domain of BRCA1 that abrogates its interaction with
351 phosphorylation-dependent binding partners (ABRA1, BRIP1 or CtIP). A second mutant
352 deleted the C-terminal coiled coil domain that is essential for HR. As expected, BRCA1
353 deletion reduced pRPA levels (Figure 5C, lane 2). Reintroduction of the BRCA1$^{S1665A}$
354 mutant allowed restoration of pRPA to almost the same extent as seen following
355 reintroduction of WT-BRCA1 (Figure 5C, compare lanes 1 and 3), suggesting that this
356 domain was not essential for the BRCA1 induced DNA damage phenotype. This finding
357 is consistent with what was observed following siRNA depletion of ABRA1, BRIP1 or
358 CtIP, whose depletion failed to abrogate BRCA1's role in promoting fork resection in the
359 absence of SCAI (Figures 5A-B). In contrast, the coiled coil domain mutant (ΔCC) of

360 BRCA1 did not fully restore pRPA (Figure 5D, compare lanes 1 & 3) suggesting that this
361 domain was important for BRCA1's role. To address this fully, we performed a dose
362 curve of HU treatment and compared the ability of the WT BRCA1 and BRCA1$^{\Delta CC}$
363 mutants to rescue SCAI dependent DNA breakage and resection (Figure 5E). These
364 data showed that the coiled coil domain of BRCA1 was required to fully orchestrate
365 damage signaling in the absence of SCAI (Figure 5E, compare lanes 4&5, 6&7, 8&9)
366 and that interaction between BRCA1 and CtIP does not account for the observed SCAI-
367 depletion phenotype.
368
369 **Preventing fork reversal upon fork stalling confers a dependency on Protexin**
370 Our data so far suggests that BRCA1 drives DNA breakage at stalled forks upon
371 replication stress. BRCA1 also has a well-established role in protecting arrested forks
372 from degradation[49]. This difference in phenotypes may result from differential
373 processing by remodeling enzymes. The fork reversal activity of the enzymes
374 SMARCAL1, ZRANB3 and HLTF represent a major mechanism of stalled fork
375 processing[6,7]. Multiple studies have shown that when fork progression is halted, fork
376 reversal by these enzymes drives the creation of a chicken-foot structure that is
377 protected from breakage and resection by BRCA1[35,36], a phenotype opposite to the
378 DNA break promoting activity of BRCA1 that we see under our conditions. We reasoned
379 that if DNA breakage seen in the absence of SCAI was occurring downstream of fork
380 reversal, it would be abolished upon depletion of fork reversal enzymes. For these
381 experiments, we have employed pRPA and γH2AX as a readout.
382 To determine whether fork reversal plays a similar role under our treatment
383 conditions, we co-depleted SCAI and either SMARCAL1 or ZRANB3. To our surprise,
384 rather than reduce damage signaling upon SCAI loss, knockdown of either SMARCAL1
385 or ZRANB3 led to consistent increases in pRPA and γH2AX upon HU treatment (Figure
386 6A, compare lanes 2, 5 & 8). The same phenotype was also seen upon co-depletion of
387 REV3 and either SMARCAL1 or ZRANB3 (Figure 6A, compare lanes 3, 6 & 9). These
388 results were further validated by knocking down SMARCAL1 with two independent
389 siRNAs, which led to similar increases in the absence of SCAI (Figure 6B, compare
390 lanes 2, 4 & 6). That this phenotype was shared between SMARCAL1 and ZRANB3
391 and was seen with multiple siRNAs against SMARCAL1 suggested that not only was
392 damage signaling and presumably DNA breakage in the absence of SCAI not occurring
393 downstream of fork reversal, but that it might also compete with fork reversal for repair
394 of stalled forks. An alternative explanation might be that DNA breaks form downstream
395 of a parallel fork reversal mechanism to that orchestrated by SMARCAL1/ZRANB3.
396 Such a parallel mechanism has been suggested to occur via FBH1[50]. To examine this,
397 we knocked down FBH1 using siRNAs. We observed that, similar to loss of
398 SMARCAL1, FBH1 depletion also led to increased pRPA and γH2AX in the absence of
399 SCAI (Figure 6C). Thus, depletion of multiple fork reversal enzymes all led to increased
400 damage signaling in the absence of Protexin. That the increased damage signaling in
401 the absence of fork reversal was more marked in the absence of Protexin suggests that
402 a SCAI/REV3-dependent process might compete with fork reversal as a mechanism for
403 stalled fork rescue. We cannot however rule out the possibility that Protexin and fork
404 reversal may act at different steps of the repair process, leading to more severe
405 phenotypes upon co-depletion.

406
407 **RAD51 activity globally regulates stalled fork metabolism**
408 RAD51 has been implicated in various fork processing roles in cells undergoing
409 replication stress. It is important for fork reversal, protecting stalled forks against the
410 activity of nucleases, and is key for recombination through template switching[51].
411 RAD51's recombination function can be genetically uncoupled from the other functions,
412 as multiple studies have shown that RAD51 strand exchange activity is not required for
413 fork protection[50,52,53]. To determine if and how RAD51 regulates the phenotypes seen in
414 the absence of SCAI/REV3, we first depleted RAD51 using a pool of siRNAs (Figure
415 S6A). Depletion of RAD51 abolished the increased pRPA and γH2AX seen in the
416 absence of SCAI (Figure S6A). We next tested RAD51's role using two independent
417 siRNAs and observe similar effects – loss of RAD51 abolished pRPA and γH2AX upon
418 HU treatment even when SCAI was absent (Figure 6D). To further determine how
419 RAD51 contributes to the increased pRPA and γH2AX seen upon fork stalling, we
420 tested the effect of inhibiting RAD51 strand exchange activity using a previously
421 described inhibitor B02[54]. Surprisingly, RAD51 inhibition completely abolished the break
422 signaling seen upon loss of SCAI or REV3 (Figure 6E, compare lanes 2&3 to lanes
423 5&6), without affecting cell cycle distribution (Figure S6B), suggesting that this function
424 requires or occurs downstream of the strand exchange activity of RAD51. We showed
425 earlier that inhibition of fork reversal led to additive increases in fork breakage upon
426 SCAI loss. We were curious whether this increase was also modulated by RAD51.
427 Remarkably, RAD51 inhibition completely prevented the increased break signaling seen
428 in the absence of SCAI when fork reversal was prevented either via SMARCAL1
429 knockdown (Figure 6F) or via PARP inhibition (Figure S6C) which has been shown to
430 modulate fork reversal outcomes[15].
431 Next, to determine how SMARCAL1 and SCAI modulated fork dynamics, we
432 performed similar DNA fiber assays as in Figure 3A. SMARCAL1 loss has been shown
433 to impair stalled-fork restart and promote replication stress associated fork
434 breakage[55,56]. Depletion of SCAI and SMARCAL1 led to additively enhanced shortening
435 of DNA fibers upon replication stress (Figure 6G, left panel). Co-depletion also led to
436 reduced lengths of restarted forks (Figure 6G, right panel), suggesting that both proteins
437 function in parallel to promote stalled fork rescue and prevent DNA breakage. Next, we
438 tested the effect of RAD51 in a similar assay. Multiple groups have shown that RAD51
439 promotes restart of stalled forks, including through strand exchange-dependent
440 mechanisms[13,52,57]. Unlike SMARCAL1, RAD51 inhibition rescued the fiber length
441 shortening seen upon SCAI loss (Figure 6H, left panel) but markedly enhanced the
442 shortening of the restarted forks (Figure 6H, right panel) suggesting that RAD51
443 promotes breakage of stalled forks but is essential for stalled fork rescue. To directly test
444 RAD51's effect on DNA break formation, we performed neutral comet assays. Upon
445 replication stress, RAD51 depletion prevented DNA break formation in the absence of
446 SCAI (Figure 6I, see also Figure S7B). Taken together these data suggests that RAD51
447 is important for formation of DNA breaks seen in the absence of Protexin, and that
448 failure of fork reversal leads to increased RAD51 driven breakage when SCAI or REV3
449 is absent.
450

451 **BRCA1-RAD51 axis governs SLX1-SLX4 and ERCC1 mediated DNA breakage**
452 **upon Protexin loss**
453 We next wanted to determine how DNA breaks form in the absence of SCAI or
454 REV3. Cells possess several structure specific nucleases that orchestrate cleavage of
455 stressed forks[17]. Among these, MUS81 has been shown to promote fork processing and
456 restart under various conditions[58,59]. Other nuclease complexes such as SLX4-SLX1
457 and XPF-ERCC1 have also been implicated [17,60]. We co-depleted SCAI or REV3 cells
458 with siRNAs against MUS81 or SLX4 following treatment with HU. We found that loss of
459 SLX4, but not MUS81, reduced γH2AX levels in SCAI depleted cells (Figure 7A). A
460 similar trend was observed in REV3 depleted cells: MUS81 had no effect or led to
461 moderate increases in γH2AX, whereas SLX4 depletion reduced γH2AX levels (Figure
462 7B). We next determined whether SLX4-associated nuclease factors, specifically SLX1
463 or ERCC1, the binding partner of the XPF1 nuclease, also contributed to the elevated
464 damage signaling caused by Protexin loss. We found reduced signaling when ERCC1
465 was knocked down and a similar but milder effect in the absence of SLX1 (Figure 7C).
466 Having consistently observed involvement of SLX4, we directly examined break
467 formation by performing neutral comet assays. As expected, SCAI depletion led to
468 increased comet tail moments which was significantly reduced by SLX4 depletion
469 (Figure 7D). Synchronization experiments revealed that this cleavage event occurred
470 prior to mitotic entry (Figure S7B).
471 We next sought to determine whether and how SLX4 was recruited to stalled
472 forks and how this was modulated by loss of SCAI. Fractionation experiments revealed
473 that SCAI loss led to increased amounts of SLX4 in the chromatin fraction compared to
474 controls (Figure 7E, compare lanes 1 & 2). We did not observe such increases with
475 MUS81 or MRE11 (Figure 7E). Strikingly, RAD51 inhibition led to significant reduction in
476 not only γH2AX levels, but also in the amount of SLX4 on chromatin (Figure 7E), and
477 the increased SLX4 amounts on chromatin seen in the absence of SCAI was prevented
478 by B02 treatment (Figure 7E, compare lanes 2 and 4). Taken together, these
479 experiments suggest that DNA breakage in the absence of SCAI/REV3 occurs
480 downstream of RAD51 strand exchange activity but likely independent of fork reversal
481 (see Figure 6).
482 To further characterize the mechanism by which stalled forks break, we depleted
483 BRCA1. Upon SCAI depletion, BRCA1 KO showed reduced chromatin levels of SLX4
484 compared to controls (Figure S7A); this finding is consistent with a prior report [61]. To
485 further examine this role, and to determine how it was modulated by RAD51, we
486 knocked down BRCA1 using siRNAs. HU treatment resulted in slightly increased
487 amounts of SLX4 on chromatin (Figure 7E, compare lanes 1 & 3). Similar to what was
488 seen following RAD51 inhibition or in BRCA1 KO cells, BRCA1 KD also resulted in
489 reduction in the amount of damage induced SLX4 on chromatin (Figure 7F, compare
490 lanes 1 & 3). Similar to what was seen following RAD51 inhibition or in BRCA1 KO cells,
491 BRCA1 KD also resulted in reduction in the amount of damage induced SLX4 on
492 chromatin (Figure 7F). Next, to determine how BRCA1 and RAD51 activities contributed
493 to DNA breakage, we examined chromatin association of RAD51 and its modulation by
494 BRCA1. Upon treatment with HU, there was increased amounts of RAD51 on chromatin
495 (Figure 7F, compare lanes 1 & 3). Loss of BRCA1 significantly prevented the increase in
496 RAD51 amounts on chromatin (Figure 7F, lane 4). Taken together these results identify

497 a BRCA1-RAD51 axis upon Protexin loss that promotes SLX4 accumulation to salvage
498 stalled replication forks.
499
500 **DISCUSSION**
501 In this work, we have uncovered a novel stalled fork maintenance mechanism requiring
502 the activities of both the fork protecting factor SCAI and the DNA polymerase REV3 to
503 prevent pathologic fork breakage upon replication stress. Our experiments reveal key
504 roles for BRCA1 and RAD51, as their loss prevented SLX4 chromatin association and
505 DNA breakage in the absence of Protexin, suggesting failure downstream of HR.
506 Supporting this, we find requirements for both the HR-promoting coiled-coil domain of
507 BRCA1 as well as the strand exchange activity of RAD51. We propose that, at certain
508 distressed forks, BRCA1-RAD51 drive fork restart that confers a dependency on the
509 SCAI/REV3 complex. Surprisingly, this process appears to occur either parallel to or
510 upstream of SMARCAL1/ZRANB3 or FBH1-mediated fork reversal, as loss of fork
511 reversal factors led to increased break signaling, additive fork shortening and enhanced
512 restart defects upon SCAI loss (model in Figure 7G).
513
514 Using multiple approaches, we show that increased break formation upon Protexin loss
515 likely occurs in S phase, supporting the conclusion that Protexin limits fork breakage.
516 Furthermore, single molecule fiber analysis revealed fork shortening upon HU treatment
517 whenever SCAI or REV3 was absent. SCAI is known to restrict EXO1 activity, yet EXO1
518 depletion did not rescue fork shortening seen in the absence of SCAI under these
519 conditions. In fact, loss of SMARCAL1, which could promote degradation of both
520 nascent strands following reversal[35,49], led to further reduction in fork lengths. The
521 observation of reduced lengths of restarted forks alongside modest reduction in restart
522 efficiency in the absence of SCAI suggest that distressed forks upon Protexin loss are
523 salvaged for inefficient restart. This is likely due to RAD51 activity[13,52] and suggests that
524 SCAI may also function downstream of strand invasion. Indeed, restart experiments
525 upon RAD51 inhibition show severely compromised fork restart efficiency whilst
526 rescuing fork length shortening seen prior to release from replication stress.
527
528 In addition to its canonical roles in regulating resection and consequent pathway choice
529 at conventional DSBs, BRCA1 has several proposed roles at stalled forks[62]. Its fork
530 protection functions are well established, occurring downstream of fork reversal. Work in
531 the literature has suggested roles for BRCA1 in stalled fork remodeling leading to fork
532 restart[11,63,64] with alternative mechanisms rescuing forks upon BRCA1 loss[65]. Our
533 experiments allow us to uncouple BRCA1's role from a fork protection function not only
534 because BRCA1 loss paradoxically prevents DNA breakage but because depletion of
535 fork reversal factors, which are necessary to provide a substrate for fork protection,
536 does not abolish the DNA break formation seen in the absence of SCAI but rather
537 increases it. We also show that this role occurs independently of or distinct from
538 BRCA1's known roles at conventional breaks, the C-terminus of BRCA1 is dispensable
539 for this function, and we directly rule out a role for BRCA1's resection partner, CtIP, in
540 promoting break formation at stalled forks.
541

542 We previously employed a Tus/Ter reporter to show that SCAI is particularly important
543 for HR promotion at stalled forks[22]. Our results here suggest that this role is important
544 for fork maintenance and efficient fork restart, and that this role occurs downstream of
545 RAD51 activity. We hypothesize that certain regions of the genome are prone to stall the
546 advancing replication fork and require SCAI and REV3 to direct fork restoration and
547 repair. The nature of such regions is not yet clear. Curiously, we observed a requirement
548 for ERCC1 in driving increased break signaling in the absence of Protexin. Such a role
549 has been shown by others[60,66] and could suggest structural blocks such as hairpins.
550 Indeed, using a fragile site reporter we found that SCAI/REV3 loss results in increased
551 breaks[22], consistent with our current findings. While SCAI and REV3 appear to function
552 in concert, they do not have overlapping roles, and loss of SCAI seemed to lead to a
553 stronger restart defect than loss of REV3. Future work will uncover under what
554 scenarios SCAI and REV3 function together and how REV3 is regulated differentially
555 from its role in translesion synthesis.
556
557 A central role for RAD51 in promoting fork restart has been proposed by others[20], and
558 the fork restart defects seen in the absence of SCAI appeared to occur downstream of
559 RAD51 activity. BRCA1 depletion did not affect SCAI recruitment to chromatin, but
560 results in significant reduction in RAD51 loading on chromatin. Whether BRCA1's role
561 here lies solely in RAD51 regulation is not yet clear. One interpretation of our data is
562 that the SCAI/REV3 mediated restart mechanism occurs in parallel with SMARCAL1
563 /ZRANB3 or FBH1 mediated fork reversal. This is supported by the finding that loss of
564 fork reversal factors like SMARCAL1 paradoxically led to increased break signaling in
565 the absence of SCAI, which could indicate that forks normally processed via fork
566 reversal are funneled into a SCAI dependent pathway that ultimately leads to collapse
567 whenever SCAI was absent. Both pathways appear to require RAD51 activity, as
568 inhibiting RAD51 prevented DNA breaks whenever SCAI and SMARCAL1 were co-
569 depleted. RAD51 has been proposed to cause a CMG helicase-containing bubble
570 ahead of annealed parental strands[57]. RAD51 could promote restart by invading newly
571 synthesized DNA ahead of the annealed fork. Under-replicated regions can then be
572 duplicated by gap-synthesis post repair. BRCA1 is not essential for fork reversal [49], but
573 may enhance RAD51 chromatin association to drive strand invasion mediated fork
574 restart. We show that SCAI is required for fork restart in this context, and in the absence
575 of SCAI, SLX4 accumulates on chromatin. One possibility is that SLX4-SLX1 and
576 ERCC1 promote cleavage of the resulting HR intermediates leading to collapse. Such
577 broken forks can be engaged by alternative means of end joining or may persist leading
578 to genomic instability and cell death. Whether the same RAD51 activity drives both
579 reversal as well as HR-mediated fork restart will be a focus of future work.
580

581 **METHODS**

582 Cell lines

583 U2OS cells were originally obtained from ATCC (HTB-96). U2OS ΔSCAI and U2OS
584 cells expressing lentiCRISPR control gRNAs (WT) were previously described[22], and
585 were passaged in McCoy's 5A medium + L-Glutamine (16600-082, Gibco). hTERT-
586 RPE1 cells were originally obtained from ATCC (CRL-4000). All RPE1 cell lines and
587 their derivatives were passaged in DMEM/F12 (1:1) medium + L-Glutamine + 15mM
588 HEPES (11330-032, Gibco). RPE1 ΔBRCA1/Δp53 (referred to as ΔBRCA1 in Figure 4)
589 was a kind gift from Dr. Alan D'Andrea[67]. RPE1 TP53$^{-/-}$ GFP PINDUCER20 (referred to
590 as "parent" in Figures S5B and S7A), RPE1 TP53$^{-/-}$ BRCA1$^{-/-}$ GFP PINDUCER20
591 (referred to as "ΔBRCA1" in Figure 5C, 5D, S5B, and S7A), RPE1 Tp53$^{-/-}$ BRCA1$^{-/-}$
592 GFP-BRCA1 PINDUCER20 (referred to as "WT" in Figures 5C, 5D, 5E and "GFP-
593 BRCA1 Rescue" in Figure S5B) and RPE1 TP53$^{-/-}$ BRCA1$^{-/-}$ GFP-BRCA1 ΔCC
594 PINDUCER20 (referred to as ΔCC) were kind gifts from Dr. Andrew Blackford and were
595 previously described[48].
596

597 Reagents and Drugs

598 Dimethyl Sulfoxide (DMSO) was from Thomas Scientific (D0231). Hydroxyurea (HU)
599 was obtained from Sigma-Aldrich (H8627-5G). Aphidicolin (APH) was from Sigma-
600 Aldrich (A4487-1ML). The TLS inhibitor JH-RE-06 was obtained from MedChemExpress
601 (HY-126214, 10mM/1mLSolution). Cisplatin was from Selleck Chemicals (S1166-50mg).
602 Rad51 inhibitor B02 was from Sigma-Aldrich (553525-25MG). Olaparib from Selleck
603 Chemicals (S1060-25mg). Colcemid was obtained from Millipore Sigma (10295892001).
604

605 Antibodies

606 The antibodies used in this work include the following: Anti-vinculin 1:1000 (Sigma-
607 Aldrich, V9131-.2ML), vinculin (7F9) 1:200 (Santa Cruz Biotechnology, sc-73614), SCAI
608 1:500 (Abcam, ab124688), Chk1 (2G1D5) 1:1000 (Cell Signaling, 2360S), P-Chk1
609 (S345) (133D3) Rabbit mAb 1:1000 (Cell Signaling, 2348S), RPA 32 kDa subunit (9H8)
610 1:200 (Santa Cruz Biotechnology, sc-56770, only used for western blots), RPA32 1:200
611 (Genetex, GTX70258, only used for IF), Rabbit x-Phospho RPA32 (S4/S8) 1:1000
612 (Bethyl, A300-245A), H2AX 1:1000 (Bethyl, A300-082A), Anti-phospho-Histone H2A.X
613 (Ser139) 1:1000 (EMD Millipore Corp., 05-636), REV7 1:200 (Santa Cruz
614 Biotechnology, sc-135977), Anti-Exonuclease 1 (EXO1) 1:1000 (Bethyl, A302-640A),
615 ORC2 1:1000 (Abcam, ab68348), BRCA1 1:1000 (EMD Millipore Corp., 07-434), 53BP1
616 1:1000 (Bethyl, A300-272A), RIF1 1:1000 (Bethyl, A300-569A), CtIP 1:1000 (Bethyl,
617 A300-488A), SmarcAL1 (A-2) 1:200 (Santa Cruz Biotechnology, sc-376377), ZRANB3
618 1:1000 (Bethyl, A303-033A), FBH1 1:1000 (Abcam, ab58881), RAD51 1:1000 (Abcam,
619 ab63801), MUS81 1:200 (Santa Cruz Biotechnology, sc-53382), SLX4 1:1000 (Bethyl,
620 A302-270A), H3 1:1000 (Cell Signaling, 9715), MRE11 1:1000 (Abcam, ab214), Goat
621 anti-Mouse IgG (H+L) Secondary Antibody, HRP 1:2500 (Invitrogen, 31430), Goat anti-
622 Rabbit IgG (H+L) Secondary Antibody, HRP 1:2500 (Invitrogen, 31460), Goat anti-
623 Rabbit IgG (H+L) Highly Cross-Adsorbed Secondary Antibody, Alexa Fluor Plus 488
624 1:300 (Invitrogen, A32731), Goat anti-Mouse IgG (H+L) Highly Cross-Adsorbed
625 Secondary Antibody, Alexa Fluor Plus 594 1:300 (Invitrogen, A32742), Goat anti-Mouse

626 IgG (H+L) Highly Cross-Adsorbed Secondary Antibody, Alexa Fluor Plus 488 1:300
627 (Invitrogen, A32723).
628
629 siRNA transfections
630 RPE1 and U2OS cells were seeded onto 6-well plates and reverse transfected with 20-
631 40nM siRNA using Lipofectamine RNAiMAX reagent (13-778-150, Invitrogen) according
632 to the manufacturer's instructions. Cells were treated 48 h after treatment with drugs as
633 indicated in the legend and processed 16 to 18 h later.
634
635 SCAI rescue experiment
636 U2OS cells were transfected with plasmids using PolyJet reagent (SignaGen,
637 SL10068B) according to the manufacturer's instructions and treated with drugs as
638 indicated in the Figure legends. SCAI was cloned into the pcDNA3.1 backbone as
639 previously described [22]. The ORF sequence of SCAI was modified to avoid being
640 identified by gRNA in ΔSCAI cells. Specifically, GCTGAAGATGAT (Ala-Glu-Asp-Asp)
641 was replaced with GCAGAGGACGAC using a site-directed mutagenesis kit (New
642 England Biolabs, E0552S).
643
644 Western blotting
645 Cells were harvested, washed with ice cold phosphate-buffered saline (PBS), and lysed
646 in SDS lysis buffer (50 mM Tris HCl pH 6.8, 100 mM NaCl, 1.7% SDS, 10 mM NaF, 7%
647 glycerol) prior to sonication. Protein content was measured using Bradford reagent
648 (23236, Life Technologies) on an Eppendorf Biophotometer. Laemmli sample buffer
649 (1610747, Bio-Rad Laboratories) was added with 20 mM DTT prior to boiling the
650 samples for 5-10 min. Whole cell lysates were analyzed using sodium dodecyl sulfate
651 gel electrophoresis (SDS-PAGE) and transferred onto nitrocellulose membranes.
652 Membranes were blocked with 5% (wt/vol) milk in Tris-buffered saline with Tween
653 (TBST) for a minimum of 30 min and then probed with the indicated antibodies. Protein
654 bands were quantified with ImageJ.
655
656 Chromatin fractionation
657 Chromatin fractions were done as previously described [68]. Briefly, RPE1 cells previously
658 transfected with the indicated siRNAs were seeded into 10 cm plates, treated with drugs
659 as indicated, then harvested and washed with ice cold PBS. Sedimented cells were
660 resuspended in cold Solution 1 (10 mM Hepes (pH 7.9), 10 mM KCl, 1.5 mM $MgCl_2$,
661 0.34 M sucrose, 1 mM DTT, 10% glycerol, 1mM $Na_3VO_4$, protease and phosphatase
662 inhibitors). Triton X-100 was added to 0.1%, and samples were incubated on ice prior to
663 centrifuging. The supernatant was removed as the cytoplasmic extract, and sedimented
664 nuclei were washed with Solution 1 prior to being lysed in Solution 2 (3 mM EDTA,
665 0.2 mM EGTA, 1 mM DTT, protease and phosphatase inhibitors) on ice. Samples were
666 centrifuged, washed with cold Solution 2, and then the chromatin-enriched pellets were
667 lysed with SDS lysis buffer. Chromatin extract samples were sonicated, and protein
668 content was measured. Sample buffer was added to all samples and boiled prior to
669 western blotting.
670
671 Cell cycle analyses

672 Cells were treated with indicated drugs for 18h prior to being harvested. Cells were then
673 washed with ice cold PBS, then fixed in 70% ethanol at 4 °C overnight. Samples were
674 pelleted, washed with ice cold PBS, and resuspended in 50 µg/mL propidium iodide
675 solution containing 0.1 mg/mL RNase A. Samples were then incubated at 37°C in the
676 dark for 15-30 min and flow cytometry was performed using a FACSymphony A5 (BD
677 Biosciences). Data were analyzed using FlowJo software.
678
679 Immunofluorescent staining for Flow Cytometry
680 RPE1 cells were reverse transfected with the indicated siRNAs as described. 48 or 64
681 hours post transfection; cells were left untreated (0 hr control) or treated with 1.5 mM
682 HU for the indicated duration. After the treatment duration, cells were harvested, fixed
683 and immuno-labelled following the protocol described by Zimmermann *et al* with minor
684 modifications. Briefly, cells were detached using trypsin, pelleted at 600 rpm for 5 min,
685 washed in 1X PBS then fixed in 1 ml of 4% PFA for 10 min at RT. The cells were again
686 pelleted as before and resuspended in 100 µl of PBS. 900 µl of prechilled (-20oC)
687 methanol was then added to the cell suspension dropwise while vortexing at the lowest
688 speed. Fixed cells were then kept at -20oC at least overnight. Next, cells were spun
689 down, washed in PBS, resuspended in blocking buffer (3% BSA in PBS) and incubated
690 for 30 minutes at room temperature. After blocking, cells were pelleted and
691 resuspended in 200 µl of dilute rabbit anti-pRPA antibody (Bethyl A300-245A; 1:750)
692 and mouse anti Phospho-H2A.X(γH2A.X) (EMD Millipore 05636IMI 1:750) in blocking
693 buffer and incubated at RT for 2 hrs. Following the 2-hour incubation, the antibody was
694 diluted by adding 2 ml of PBS and cells spun down. The supernatant was carefully
695 removed, and the pellet resuspended in 200 µl of dilute Alexa Fluor 488-conjugated
696 goat anti-rabbit antibody and Alexa Fluor594- conjugated anti-mouse (Molecular
697 Probes/Thermo Fisher, 1:1,000) in blocking buffer then incubated at RT for 1 hour. The
698 cells were washed by adding 2 ml of PBS and centrifuging for 5 minutes. The pellet was
699 resuspended in 1 µg/ml DAPI incubated for 15 minutes and samples analyzed on the
700 FACSymphony A3 (BD Biosciences). Data was acquired using the BD FACSDiva
701 software and analyzed using FlowJo.
702
703 Clonogenic survival assays
704 Cells were transfected as stated above for 48 h with the indicated siRNAs and then
705 treated with indicated doses of drugs for 18 h. The number of cells plated in six-well
706 plates was adjusted based on the dose of drug the cells were exposed to. Cells were
707 allowed to form colonies for 10-14 days prior to being fixed and stained using Crystal
708 Violet. Analyses were performed using ImageJ.
709
710 Immunofluorescence Assay
711 Cells were transfected with the indicated siRNAs as above and plated onto glass
712 coverslips 18 h later. 48 h after the transfection, the cells were treated with HU for the
713 indicated dose and duration. The cells were then washed with ice-cold PBS on ice, pre-
714 extracted for 5 min on ice using cytoskeleton buffer (100 mM NaCl, 10 mM HEPES (pH
715 7.8), 3 mM $MgCl_2$, 300 mM sucrose, 0.1% Triton X-100), fixed with 4%
716 paraformaldehyde in PBS for 10 min at room temp and then permeabilized with 0.5%
717 Triton-100 in 1X PBS. Samples were then blocked with 3% bovine serum albumin (BSA)

718 in PBS for a minimum of 30 min on a rocker followed by overnight incubation with
719 primary antibodies at 4 °C in a humidified chamber. Unbound primary antibodies were
720 washed using 3% BSA in PBS and then samples incubated with secondary antibody for
721 1 h at RT in the dark. Unbound antibody was washed with PBS and then samples
722 stained with 1 μg/ml DAPI for 1 h before mounting the coverslips on a microscope slide
723 for imaging. Images were acquired using an LSM 780 NLO (Zeiss), and a minimum of
724 100 nuclei for each group were analyzed using ImageJ.
725
726 Proximity Ligation Assay:
727 RPE cells were reverse transfected with the indicated siRNAs. 24h later cells were
728 replated on coverslips and treated with drugs as indicated. Coverslips were washed
729 once with 1xPBS, and pre-extracted with CSK (100nM NaCl, 100mM HEPES pH 7.8,
730 3mM MgCl2, 300mM Sucrose, 0.1% TritonX-100) for 5min on ice and then with
731 CSK+0.5% TritonX-100 for 5min on ice. Samples were fixed with 100% Methanol for
732 20min at -20°C. Coverslips blocked with 5% BSA at room temperature for at least 1 hr.
733 Indicated primary antibodies were incubated overnight at 4°C in a humid chamber,
734 washed with 1xPBS. Subsequent steps were performed according to the manufacturer's
735 (Duolink®, Sigma) instructions. Briefly, cells were incubated with secondary PLA probes
736 (Duolink® In Situ PLA® Probe Anti- Rabbit PLUS (DUO92002), Duolink® In Situ PLA®
737 Probe Anti-Mouse MINUS (DUO92004) in antibody diluent) for 1h at 37°C in a humid
738 chamber, washed twice with Wash Buffer A (10mM Tris Base, 150mM NaCl, 0.05%
739 Tween-20, pH=7.4) and then incubated with Duolink® In Situ Detection Reagents Red,
740 first with the ligation mix for 30min at 37°C in a humid chamber. Cells were then washed
741 twice with 1mL Wash Buffer A and incubated with PLA amplification for 100min at 37°C
742 in a humid chamber. Coverslips were washed with Wash Buffer B (200mM Tris Base,
743 100mM NaCl, pH 7.4) and then 0.01x Wash Buffer B before being sealed with DAPI in
744 mounting media (SouthernBiotech, DAPI Fluoromont-G, 0100-20). PLA foci were
745 imaged with a 40x oil objective on a Zeiss 780 confocal microscope. Images were taken
746 as 10x0.52μm Z-stacks to ensure the entire nucleus was imaged, and projected using
747 FIJI sum slices for intensity and count analysis. Representative images were max
748 projections.
749
750 QIBC image acquisition and analysis
751 Fixed and stained slides were imaged on a Molecular Devices ImageXpress Microscope
752 equipped with a Nikon 40x/0.95 PlanApo objective. Around 2000 nuclei were acquired
753 for each condition. Quantification was then performed using the "Multi Wavelength Cell
754 Scoring" module in the MetaXpress software. Briefly, nuclei were segmented using the
755 DAPI channel, and the raw Mean Fluorescent Intensities (MFIs) of each nucleus were
756 measured for DAPI, RPA (AF488), and gamma-H2AX (AF594). All cells were then
757 plotted for each condition and p-values generated by Ordinary one-way ANOVA,
758 Tukey's multiple comparison test
759
760 DNA fiber assays
761 hTERT-RPE1 cells were reverse transfected with the indicated siRNAs at 20 nM using
762 Lipofectamine RNAiMAX reagent (Invitrogen). Transfected hTERT-RPE1 cells were
763 pulse-labeled with CldU followed by IdU as indicated in each Figure. After being labeled,

764 cells were harvested and embedded in 0.6% low melting point agarose gel plugs. Cells
765 in plugs were incubated with lysis solution (0.2 M EDTA, 0.5% SDS, 3 mg/mL
766 Proteinase K) overnight at 50°C. Each plug was dissolved in 0.5 M MES solution (pH
767 5.5) by β-agarase (NEB) overnight treatment and DNA was attached to a pre-treated
768 coverslip (PolyAn) using FiberComb® Molecular Combing System (GENOMIC VISION).
769 DNA on coverslips was denatured by incubating in denaturing solution (0.5 N NaOH, 1
770 M NaCl) for 8 min. Blocking was performed with 5% BSA in PBS for 60 min. For
771 immunostaining, coverslips were incubated overnight with primary antibodies; ab6326
772 anti-BrdU (cross-reacts with CldU) antibody (rat) (1:50) and BD Biosciences 347580
773 anti-BrdU (cross-reacts with IdU) antibody (mouse) (1:8). Slides were washed with PBS
774 followed by incubation for one hour with the secondary antibodies; anti-rat Alexa-488
775 antibody (1:300) and anti-mouse Alexa-594 antibody (1:300). After wash with PBS,
776 coverslips were mounted onto glass slides with anti-fade mounting medium
777 (SlowFade™ Glass Soft-Set Antifade Mountant, Invitrogen). Images were acquired with
778 Leica STELLARIS confocal microscope. DNA fiber numbers and lengths were manually
779 analyzed using LAS X software (Leica Microsystems).
780
781 Metaphase spreads
782 hTERT-RPE1 cells were reverse transfected with the indicated siRNAs as above using
783 Lipofectamine RNAiMAX. Two days after the transfection, cells were treated with 2 mM
784 HU or PBS for 18 h, followed by PBS wash and 24 h incubation in normal medium.
785 Cells were exposed to colcemid (100 ng/ml) for the last 3 h of the 24 h normal medium
786 incubation before harvest. Collected cells were treated with a hypotonic solution (1:2
787 mixture of 0.075 M KCl and 0.9% Na citrate) for 10 min and fixed with 3:1 methanol:
788 acetic acid. Fixed cells were transferred on glass slides dropwise, and the slides were
789 stained with Giemsa stain. Cells in metaphase were observed using a Zeiss Axiovert
790 200M microscope and captured using AxioVision. Over 50 metaphase cells were
791 analyzed per sample.
792
793 Neutral Comet assay
794 hTERT-RPE1 cells were incubated with 2 mM Thymidine for 16 h followed by reverse
795 transfection with indicated siRNAs at 20 nM using Lipofectamine RNAiMAX reagent
796 (Invitrogen). Eight hour after the end of the first Thymidine incubation, cells were
797 incubated with 2mM Thymidine again for 16 h. HU 2 mM treatment started 2 h after the
798 end of the second Thymidine incubation. Cells were harvested 24 h later for Comet
799 assay. Alternatively, hTERT-RPE1 or U2OS cells were reverse transfected as above
800 then, two days after the transfection, treated with 2 mM HU or PBS for 40 h. After HU
801 treatment, cells were harvested and resuspended in ice-cold PBS. 10μL of the cell
802 suspension was mixed with 100 μL of melted 0.7% low melting point agarose gel, and
803 the mixture was spread onto a pre-coated CometSlide™ (R&D SYSTEMS®). After the
804 agarose gel was solidified at 4 °C, the slide was immersed in lysis solution (10 mM Tris
805 base, 2.5 M NaCl, 100 mM $Na_2$-EDTA, 10% DMSO, 1% Triton X-100, pH 10) for 2 h at 4
806 °C followed by a 30 min incubation in neutral electrophoresis buffer (100 mM Tris base,
807 300 mM sodium acetate, pH 9). Then, the slide was placed in an electric field for 40
808 min. After the electrophoresis, the slide was immersed in DNA precipitation solution
809 (82% ethanol, 1 mM ammonium acetate) for 30 min followed by a 30 min incubation in

810 70% ethanol. SYBR Gold dye (Invitrogen) was used to stain DNA (“comet”) and images
811 were obtained with TissueFAXS (TissueGnostics). Comets were analyzed with ImageJ
812 (OpenComet).
813
814 Quantification and statistical analyses
815 Statistical analyses were performed using Prism 10 (GraphPad). All statistics used are
816 indicated in the Figure legends. For all experiments: n.s. $P \geq 0.05$; *$P<0.05$; **$P < 0.01$;
817 ***$P < 0.001$; ****$P<0.0001$. All experiments in this work were performed multiple
818 independent times with similar results. Multiple siRNAs, multiple knockout clones, and
819 multiple cell lines were analyzed to confirm that results were not caused by off-target
820 effects or clonal variations. Representative images and/or experiments are shown for
821 westerns, cell cycle analyses, DNA fiber assays and IFs.
822
823

824 **REFERENCES AND NOTES**
825


826 1. Zeman, M.K. & Cimprich, K.A. Causes and consequences of replication stress.
827 *Nat Cell Biol* **16**, 2-9 (2014).
828 2. Ciccia, A. & Elledge, S.J. The DNA damage response: making it safe to play with
829 knives. *Mol Cell* **40**, 179-204 (2010).
830 3. Saxena, S. & Zou, L. Hallmarks of DNA replication stress. *Mol Cell* **82**, 2298-
831 2314 (2022).
832 4. Gaillard, H., Garcia-Muse, T. & Aguilera, A. Replication stress and cancer. *Nat*
833 *Rev Cancer* **15**, 276-89 (2015).
834 5. Cimprich, K.A. & Cortez, D. ATR: an essential regulator of genome integrity. *Nat*
835 *Rev Mol Cell Biol* **9**, 616-27 (2008).
836 6. Neelsen, K.J. & Lopes, M. Replication fork reversal in eukaryotes: from dead end
837 to dynamic response. *Nat Rev Mol Cell Biol* **16**, 207-20 (2015).
838 7. Quinet, A., Lemacon, D. & Vindigni, A. Replication Fork Reversal: Players and
839 Guardians. *Mol Cell* **68**, 830-833 (2017).
840 8. Schlacher, K. et al. Double-strand break repair-independent role for BRCA2 in
841 blocking stalled replication fork degradation by MRE11. *Cell* **145**, 529-42 (2011).
842 9. Errico, A. & Costanzo, V. Mechanisms of replication fork protection: a safeguard
843 for genome stability. *Crit Rev Biochem Mol Biol* **47**, 222-35 (2012).
844 10. Petermann, E. & Helleday, T. Pathways of mammalian replication fork restart. *Nat*
845 *Rev Mol Cell Biol* **11**, 683-7 (2010).
846 11. Scully, R., Elango, R., Panday, A. & Willis, N.A. Recombination and restart at
847 blocked replication forks. *Curr Opin Genet Dev* **71**, 154-162 (2021).
848 12. Zellweger, R. et al. Rad51-mediated replication fork reversal is a global response
849 to genotoxic treatments in human cells. *J Cell Biol* **208**, 563-79 (2015).
850 13. Petermann, E., Orta, M.L., Issaeva, N., Schultz, N. & Helleday, T. Hydroxyurea-
851 stalled replication forks become progressively inactivated and require two
852 different RAD51-mediated pathways for restart and repair. *Mol Cell* **37**, 492-502
853 (2010).
854 14. Mouron, S. et al. Repriming of DNA synthesis at stalled replication forks by
855 human PrimPol. *Nat Struct Mol Biol* **20**, 1383-9 (2013).
856 15. Berti, M. et al. Human RECQ1 promotes restart of replication forks reversed by
857 DNA topoisomerase I inhibition. *Nat Struct Mol Biol* **20**, 347-54 (2013).
858 16. Pepe, A. & West, S.C. MUS81-EME2 promotes replication fork restart. *Cell Rep*
859 **7**, 1048-55 (2014).
860 17. Sarbajna, S., Davies, D. & West, S.C. Roles of SLX1-SLX4, MUS81-EME1, and
861 GEN1 in avoiding genome instability and mitotic catastrophe. *Genes Dev* **28**,
862 1124-36 (2014).
863 18. Kockler, Z.W., Osia, B., Lee, R., Musmaker, K. & Malkova, A. Repair of DNA
864 Breaks by Break-Induced Replication. *Annu Rev Biochem* **90**, 165-191 (2021).
865 19. Kramara, J., Osia, B. & Malkova, A. Break-Induced Replication: The Where, The
866 Why, and The How. *Trends Genet* **34**, 518-531 (2018).
867 20. Ait Saada, A., Lambert, S.A.E. & Carr, A.M. Preserving replication fork integrity
868 and competence via the homologous recombination pathway. *DNA Repair (Amst)*
869 **71**, 135-147 (2018).

870 21. Chakraborty, S., Schirmeisen, K. & Lambert, S.A. The multifaceted functions of
871 homologous recombination in dealing with replication-associated DNA damages.
872 *DNA Repair (Amst)* **129**, 103548 (2023).
873 22. Adeyemi, R.O. et al. The Protexin complex counters resection on stalled forks to
874 promote homologous recombination and crosslink repair. *Mol Cell* **81**, 4440-4456
875 e7 (2021).
876 23. Hansen, R.K. et al. SCAI promotes DNA double-strand break repair in distinct
877 chromosomal contexts. *Nat Cell Biol* **18**, 1357-1366 (2016).
878 24. Ikegami, S. et al. Aphidicolin prevents mitotic cell division by interfering with the
879 activity of DNA polymerase-alpha. *Nature* **275**, 458-60 (1978).
880 25. Macheret, M. & Halazonetis, T.D. DNA replication stress as a hallmark of cancer.
881 *Annu Rev Pathol* **10**, 425-48 (2015).
882 26. Gan, G.N., Wittschieben, J.P., Wittschieben, B.O. & Wood, R.D. DNA polymerase
883 zeta (pol zeta) in higher eukaryotes. *Cell Res* **18**, 174-83 (2008).
884 27. Makarova, A.V. & Burgers, P.M. Eukaryotic DNA polymerase zeta. *DNA Repair*
885 *(Amst)* **29**, 47-55 (2015).
886 28. Ware, R.E. & Dertinger, S.D. Absence of hydroxyurea-induced mutational effects
887 supports higher utilisation for the treatment of sickle cell anaemia. *Br J Haematol*
888 **194**, 252-266 (2021).
889 29. Zhao, L. & Washington, M.T. Translesion Synthesis: Insights into the Selection
890 and Switching of DNA Polymerases. *Genes (Basel)* **8**(2017).
891 30. Wojtaszek, J.L. et al. A Small Molecule Targeting Mutagenic Translesion
892 Synthesis Improves Chemotherapy. *Cell* **178**, 152-159 e11 (2019).
893 31. Celis, J.E. & Celis, A. Cell cycle-dependent variations in the distribution of the
894 nuclear protein cyclin proliferating cell nuclear antigen in cultured cells:
895 subdivision of S phase. *Proc Natl Acad Sci U S A* **82**, 3262-6 (1985).
896 32. Krakoff, I.H., Brown, N.C. & Reichard, P. Inhibition of ribonucleoside diphosphate
897 reductase by hydroxyurea. *Cancer Res* **28**, 1559-65 (1968).
898 33. Sirbu, B.M. et al. Analysis of protein dynamics at active, stalled, and collapsed
899 replication forks. *Genes Dev* **25**, 1320-7 (2011).
900 34. Toledo, L.I. et al. ATR prohibits replication catastrophe by preventing global
901 exhaustion of RPA. *Cell* **155**, 1088-103 (2013).
902 35. Kolinjivadi, A.M. et al. Smarcal1-Mediated Fork Reversal Triggers Mre11-
903 Dependent Degradation of Nascent DNA in the Absence of Brca2 and Stable
904 Rad51 Nucleofilaments. *Mol Cell* **67**, 867-881 e7 (2017).
905 36. Vujanovic, M. et al. Replication Fork Slowing and Reversal upon DNA Damage
906 Require PCNA Polyubiquitination and ZRANB3 DNA Translocase Activity. *Mol*
907 *Cell* **67**, 882-890 e5 (2017).
908 37. Lemay, J.F. et al. A genome-wide screen identifies SCAI as a modulator of the
909 UV-induced replicative stress response. *PLoS Biol* **20**, e3001543 (2022).
910 38. Densham, R.M. & Morris, J.R. Moving Mountains-The BRCA1 Promotion of DNA
911 Resection. *Front Mol Biosci* **6**, 79 (2019).
912 39. Tarsounas, M. & Sung, P. The antitumorigenic roles of BRCA1-BARD1 in DNA
913 repair and replication. *Nat Rev Mol Cell Biol* **21**, 284-299 (2020).
914 40. Baer, R. & Ludwig, T. The BRCA1/BARD1 heterodimer, a tumor suppressor
915 complex with ubiquitin E3 ligase activity. *Curr Opin Genet Dev* **12**, 86-91 (2002).

41. Bouwman, P. et al. 53BP1 loss rescues BRCA1 deficiency and is associated with triple-negative and BRCA-mutated breast cancers. *Nat Struct Mol Biol* **17**, 688-95 (2010).
42. Kostyrko, K., Bosshard, S., Urban, Z. & Mermod, N. A role for homologous recombination proteins in cell cycle regulation. *Cell Cycle* **14**, 2853-61 (2015).
43. Savage, K.I. & Harkin, D.P. BRCA1, a 'complex' protein involved in the maintenance of genomic stability. *FEBS J* **282**, 630-46 (2015).
44. Wang, B. et al. Abraxas and RAP80 form a BRCA1 protein complex required for the DNA damage response. *Science* **316**, 1194-8 (2007).
45. Cruz-Garcia, A., Lopez-Saavedra, A. & Huertas, P. BRCA1 accelerates CtIP-mediated DNA-end resection. *Cell Rep* **9**, 451-9 (2014).
46. Yun, M.H. & Hiom, K. CtIP-BRCA1 modulates the choice of DNA double-strand-break repair pathway throughout the cell cycle. *Nature* **459**, 460-3 (2009).
47. Wu, X. & Wang, B. Abraxas suppresses DNA end resection and limits break-induced replication by controlling SLX4/MUS81 chromatin loading in response to TOP1 inhibitor-induced DNA damage. *Nat Commun* **12**, 4373 (2021).
48. Tsukada, K. et al. BLM and BRCA1-BARD1 coordinate complementary mechanisms of joint DNA molecule resolution. *Mol Cell* **84**, 640-658 e10 (2024).
49. Taglialatela, A. et al. Restoration of Replication Fork Stability in BRCA1- and BRCA2-Deficient Cells by Inactivation of SNF2-Family Fork Remodelers. *Mol Cell* **68**, 414-430 e8 (2017).
50. Liu, W., Krishnamoorthy, A., Zhao, R. & Cortez, D. Two replication fork remodeling pathways generate nuclease substrates for distinct fork protection factors. *Sci Adv* **6**(2020).
51. Bhat, K.P. & Cortez, D. RPA and RAD51: fork reversal, fork protection, and genome stability. *Nat Struct Mol Biol* **25**, 446-453 (2018).
52. Mason, J.M., Chan, Y.L., Weichselbaum, R.W. & Bishop, D.K. Non-enzymatic roles of human RAD51 at stalled replication forks. *Nat Commun* **10**, 4410 (2019).
53. Halder, S. et al. Double-stranded DNA binding function of RAD51 in DNA protection and its regulation by BRCA2. *Mol Cell* **82**, 3553-3565 e5 (2022).
54. Huang, F. et al. Identification of specific inhibitors of human RAD51 recombinase using high-throughput screening. *ACS Chem Biol* **6**, 628-35 (2011).
55. Betous, R. et al. SMARCAL1 catalyzes fork regression and Holliday junction migration to maintain genome stability during DNA replication. *Genes Dev* **26**, 151-62 (2012).
56. Ciccia, A. et al. The SIOD disorder protein SMARCAL1 is an RPA-interacting protein involved in replication fork restart. *Genes Dev* **23**, 2415-25 (2009).
57. Liu, W. et al. RAD51 bypasses the CMG helicase to promote replication fork reversal. *Science* **380**, 382-387 (2023).
58. Lai, X. et al. MUS81 nuclease activity is essential for replication stress tolerance and chromosome segregation in BRCA2-deficient cells. *Nat Commun* **8**, 15983 (2017).
59. Mayle, R. et al. DNA REPAIR. Mus81 and converging forks limit the mutagenicity of replication fork breakage. *Science* **349**, 742-7 (2015).
60. Betous, R. et al. DNA replication stress triggers rapid DNA replication fork breakage by Artemis and XPF. *PLoS Genet* **14**, e1007541 (2018).

962 61. Xu, Y. et al. 53BP1 and BRCA1 control pathway choice for stalled replication
963 restart. *Elife* **6**(2017).
964 62. Rickman, K. & Smogorzewska, A. Advances in understanding DNA processing
965 and protection at stalled replication forks. *J Cell Biol* **218**, 1096-1107 (2019).
966 63. Daza-Martin, M. et al. Isomerization of BRCA1-BARD1 promotes replication fork
967 protection. *Nature* **571**, 521-527 (2019).
968 64. Deshpande, M. et al. Error-prone repair of stalled replication forks drives
969 mutagenesis and loss of heterozygosity in haploinsufficient BRCA1 cells. *Mol*
970 *Cell* **82**, 3781-3793 e7 (2022).
971 65. Cybulla, E. et al. A RAD18-UBC13-PALB2-RNF168 axis mediates replication fork
972 recovery in BRCA1-deficient cancer cells. *Nucleic Acids Res* **52**, 8861-8879
973 (2024).
974 66. Elango, R. et al. The structure-specific endonuclease complex SLX4-XPF
975 regulates Tus-Ter-induced homologous recombination. *Nat Struct Mol Biol* **29**,
976 801-812 (2022).
977 67. Lim, K.S. et al. USP1 Is Required for Replication Fork Protection in BRCA1-
978 Deficient Tumors. *Mol Cell* **72**, 925-941 e4 (2018).
979 68. Tischler, J.D. et al. FLIP(C1orf112)-FIGNL1 complex regulates RAD51 chromatin
980 association to promote viability after replication stress. *Nat Commun* **15**, 866
981 (2024).
982
983

**Acknowledgements**
We thank all the members of the Adeyemi laboratory for advice and helpful discussions. We thank Dr. Blackford and Dr. Setiaputra for providing reagents.

**Funding**
This work was supported by NIH NIGMS R35 GM150532-01 and an Early Career Investigator Grant from the Ovarian Cancer Research Alliance (ECIG-2023-3-1004) (to ROA). R.B. was supported by a Washington Research Foundation fellowship. This research was also supported by the Cellular Imaging Shared Resource RRID:SCR_022609 and the Flow Cytometry Shared Resource, RRID:SCR_022613, of the Fred Hutch / University of Washington / Seattle Children's Cancer Consortium (P30 CA015704).

**Author Contributions**
Conceptualization: R.O.A., Methodology: C.U., H.T., R.B., S.K., X.J., R.O.A., Investigation: C.U., H.T., R.B., S.K., X.J., R.O.A., Visualization: C.U., H.T., R.B., S.K., X.J., R.O.A., Supervision: R.O.A., Writing—original draft: R.O.A., Writing—review & editing: C.U., H.T., R.B., S.K., X.J., R.O.A.

**Competing Interests**
The authors declare that they have no competing interests.

**Data and Materials Availability**
All data needed to evaluate the conclusions in the paper are present in the paper and/or the Supplementary Materials. Materials resulting from the findings of this study are available from the corresponding author upon request.

1011 **MAIN FIGURE LEGENDS**
1012
1013 **Figure 1: Protexin complex prevents DNA breakage and genomic instability**
1014 **following replication stress**
1015 **A.** WT RPE1 cells transfected with the indicated siRNAs for 60 h, then treated with 2
1016 mM hydroxyurea (HU) for 18 h, harvested, and processed for western blotting with the
1017 specified antibodies. ND, no drug, n = 3 independent experiments. **B.** Western blots
1018 (WB) from WT and SCAI-null U2OS cell lines treated with 1 mM HU for 18 h, n = 3
1019 independent experiments. **C.** WT and ∆SCAI U2OS cells were transfected with either
1020 backbone plasmids (Vector) or plasmids expressing SCAI that is resistant to
1021 CRISPR/Cas9 editing. After 30 h, cells were treated with 1.5 mM HU for another 18 h
1022 before immunoblotting. n = 3 independent experiments. **D.** WT RPE1 cells were
1023 transfected with the indicated siRNAs, then treated with vehicle (DMSO), 1 μM, or 2 μM
1024 aphidicolin (APH) for 18 h before being processed for western blotting with the specified
1025 antibodies. n = 3 independent experiments. **E.** WT RPE1 cells were transfected with the
1026 indicated siRNAs, then treated with 1 mM HU for 18 h and assayed for the indicated
1027 proteins by WB. γH2AX values are normalized to vinculin loading control. n = 3
1028 independent experiments. **F.** Top: Schematic of cell treatment protocol. Bottom:
1029 Numbers of chromosomal aberrations per metaphase cell. hTERT-RPE1 cells treated
1030 with 2 mM HU for 18 h followed by washout of HU and 24 h incubation in normal
1031 medium. Indicated siRNAs were transfected two days before HU treatment. n = 3
1032 independent experiments, mean ± S.D. Ordinary one-way ANOVA followed by Tukey's
1033 multiple comparison test. ns – not significant (P ≥ 0.05). **G.** Representative images of
1034 (**F**). Red arrow – chromosomal aberrations. **H-I.** Comet assay of WT RPE1 (**H**) and
1035 U2OS (**I**) cells treated with 2 mM HU for 40 h. Representative comets are shown on the
1036 right. Indicated siRNAs were transfected two days before HU treatment. Red line
1037 represents median, n = 3 independent experiments, representative experiment shown.
1038 Mann-Whitney test. ****P < 0.0001.
1039
1040 **Figure 2: SCAI/REV3 prevent DNA breakage in S phase**
1041 **A.** Representative IF images showing increased γH2AX in PCNA positive compared to
1042 PCNA negative RPE cells 8 h after treatment with 1.5 mM HU. Cells were transfected
1043 with control or SCAI siRNA 2 days prior. Scale bars indicate 50 micron. **B.** Plot showing
1044 the observed overlap between γH2AX and PCNA staining from (**A**), n = 2 independent
1045 experiments, with >180 cells/condition per experiment. Expected values were obtained
1046 by multiplying γH2AX and PCNA positive fractions. **C.** RPE1 cells were synchronized by
1047 double thymidine block, released for 2 h and treated with 2 mM HU for the time points
1048 shown prior to immunoblotting. Representative experiment shown, n = 2 independent
1049 experiments. **D.** Representative scatter plots showing time course changes in cell cycle
1050 distribution and level of γH2AX (left panel) or pRPA (right panel) in RPE1 cells
1051 transfected with control or siRNA targeting SCAI then treated with 1.5 mM HU for the
1052 indicated duration. The percentage of cells with high pRPA and γH2AX signals is
1053 indicated in each panel. **E.** Quantification (mean ± SEM) of three experiments as in (**D**),
1054 unpaired t-test, n = 3 independent experiments. *P=0.0332, **P = 0.002. **F.** Multivariate
1055 scatter plots from QIBC analysis showing changes in cell cycle distribution and level of
1056 γH2AX (top panel) and chromatin-bound RPA2 (bottom panel) in RPE1 cells transfected

1057 with either control, or siRNA targeting SCAI or REV3 then treated with 1.5 mM HU for
1058 16h. Top panel: untreated control (light blue), HU treated (yellow). Bottom panel:
1059 Untreated control (navy blue), HU treated (green). The numbers on the plots show the
1060 percentage of HU treated cells whose γH2AX or chromatin bound RPA2 was above the
1061 baseline in the no drug controls. **G**. Representative microscopy images showing
1062 increased chromatin bound RPA (green) and γH2AX (red) upon Protexin loss. Scale bar
1063 indicates 25 micron. **H-I**. Quantification of the integrated fluorescent intensity of RPA (**H**)
1064 and γH2AX (**I**). Red bar indicates mean and SEM of about 2000 nuclei. ****P < 0.0001,
1065 ANOVA followed by Tukey's.
1066
1067 **Figure 3: Protexin complex is required to maintain fork integrity during replication**
1068 **stress**
1069 **A.** Schematic of pulse-labeling DNA strands and representative images of two-color
1070 DNA fibers. DNA fibers were from RPE1 cells transfected with siRNAs as indicated. **B.**
1071 Lengths of two-color DNA fibers from (**A**). Green portion quantified in left panel and red
1072 (restarted) portion on right. **C.** Percentage of restarted forks (dual-labeled) over total
1073 amounts of green labeled forks from experiment in **A**, n = 3 independent experiments,
1074 unpaired t-test, **P = 0.0075 **D.** Top**,** Schematic of pulse-labeling DNA strands. **B, D-E**.
1075 Red line represents median, three independent experiments, representative experiment
1076 shown. Mann Whitney test for two group comparison and Kruskal-Wallis followed by
1077 Dunn's multiple comparison test for more than three group comparison. ns – not
1078 significant, *P < 0.05, **P < 0.01, ***P < 0.001, ****P < 0.0001.
1079
1080 **Figure 4: BRCA1 promotes S-phase DNA break formation upon Protexin loss**
1081 **A.** WT and BRCA1 null RPE1 cells were transfected with the indicated siRNAs, then
1082 treated with 1 mM HU for 18 h prior to blotting for the indicated proteins. Representative
1083 experiment shown, n = 3 independent experiments. **B.** WT and BRCA1-null RPE1 cells
1084 were transfected with the indicated siRNAs. Cells were then treated with 1 mM HU for
1085 18 h before immunoblotting against the indicated proteins. Representative experiment
1086 shown, n = 3 independent experiments. **C-D.** Representative IF images showing RPA
1087 foci (**C**) and γH2AX foci (**D**) in WT RPE1 cells following treatment with the indicated
1088 siRNAs. Cells were treated with 1.5 mM HU for 18 h prior to IF. Scale bars indicate 5
1089 micron. Quantification shown to the right. Red line represents median. **** P < 0.0001,
1090 *P = 0.0337, unpaired Welch's t test (two-tailed). **E.** Comet assay of RPE1 cells treated
1091 with 2 mM HU for 40 h. Representative comets are shown on the bottom. Indicated
1092 siRNAs were transfected two days before HU treatment. Red line represents median, n
1093 = 2 independent experiments, representative experiment shown. Kruskal-Wallis
1094 followed by Dunn's multiple comparison test. ****P < 0.0001, ns – not significant. **F-H.**
1095 Representative flow cytometry of WT and BRCA1-null RPE1 cells treated with 1.5 mM
1096 HU for 16 h. Indicated siRNAs were transfected two days before HU treatment.
1097 Percentage of cells with high pRPA and γH2AX signals is indicated in each panel.
1098 Quantification of percentage of cells with high pRPA (**G**) and γH2AX (**H**), n = 4
1099 independent experiments. **P = 0.0067, *P = 0.0307, unpaired Welch's t test (two-
1100 tailed).
1101

1102 **Figure 5: BRCA1 binding to CtIP is not required for damage signaling upon SCAI**
1103 **loss**
1104 **A.** WT RPE1 cells were transfected with the indicated siRNAs, then treated with 1 mM
1105 HU for 18 h and assayed for the indicated proteins by WB. Representative experiment
1106 shown, n = 3 independent experiments. **B.** Western blots from WT and SCAI-null U2OS
1107 cell lines transfected with the indicated siRNAs and then treated with 1.5 μM cisplatin for
1108 18 h. Representative experiment shown, n = 3 independent experiments. **C.** GFP-WT-
1109 BRCA1 rescue (labeled WT), BRCA1-null (Δ), and GFP-BRCA1-S1655 (S1655) RPE1
1110 cells were transfected with the indicated siRNAs, then treated with 2 mM HU for 18 h.
1111 WCLs were assayed for the indicated proteins by WB. Representative experiment
1112 shown, n = 3 independent experiments. **D.** GFP-WT-BRCA1 rescue (WT), BRCA1-null
1113 (Δ), and GFP-BRCA1-ΔCC (ΔCC) RPE1 cells were transfected with the indicated
1114 siRNAs, then treated with 2 mM HU for 18 h and assayed for the indicated proteins by
1115 WB. Representative experiment shown, n = 3 independent experiments. **E.** Western
1116 blots from GFP-WT-BRCA1 rescue (WT), and GFP-BRCA1-ΔCC (ΔCC) RPE1 cell lines
1117 transfected with the indicated siRNAs and treated with ND, 0.75 mM, 1.5 mM, or 3 mM
1118 HU for 18 h. Representative experiment shown, n = 3 independent experiments.
1119
1120 **Figure 6: Both Protexin and reversal factors limit breaks upon replication stress**
1121 **A.** Western blots from WT RPE1 cells transfected with the indicated siRNAs and then
1122 treated with 1 mM HU for 18 h, n = 3 independent experiments. **B.** WT RPE1 cells were
1123 transfected with the indicated siRNAs, then treated with 1 mM HU for 18 h and assayed
1124 for the indicated proteins by WB, n = 2 independent experiments. **C.** WT RPE1 cells
1125 were transfected for and treated with 1 mM HU for 18 h. WCLs were prepared, and WB
1126 were performed against the indicated proteins, n = 3 independent experiments. **D.**
1127 Western blots from WT RPE1 cells transfected with the indicated siRNAs and then
1128 treated with 2 mM HU for 18 h, n = 2 independent experiments. **E.** Western blots
1129 against the indicated proteins from WT RPE1 cells transfected, then pretreated with 27
1130 μM RAD51 inhibitor B02 or vehicle (DMSO) for 30 m and treated with 1 mM HU for 18
1131 h, n = 3 independent experiments. **F.** Western blots from WT RPE1 cells transfected
1132 with the indicated siRNAs, pretreated with 27 μM RAD51 inhibitor B02 or vehicle
1133 (DMSO) for 30 min, then treated with 1 mM HU for 18 h. n = 3 independent
1134 experiments. **G-H**. Top: schematic of pulse-labeling DNA strands. Bottom: DNA fibers
1135 were from RPE1 cells transfected with siRNAs and/or treated with B02 or vehicle as
1136 indicated. Red or Green portions of dual-labeled fibers were quantified and plotted as
1137 shown. Outliers were filtered using ROUT in Prism, ordinary one-way ANOVA followed
1138 by Tukey's. ns – not significant, *P < 0.05, **P < 0.01, ***P < 0.001, ****P < 0.0001 **I.**
1139 Comet assay of hTERT-RPE1 cells treated with 2 mM HU for 40 h. Representative
1140 comets shown at the top. Indicated siRNAs were transfected two days before HU
1141 treatment. Red line represents median, n = 3 independent experiments,
1142 representative experiment shown. Mann Whitney test, ****P < 0.0001.
1143
1144 **Figure 7: BRCA1-RAD51 axis regulate SLX1-SLX4 and ERCC1 mediated DNA**
1145 **breakage upon Protexin loss**
1146 **A.** WT RPE1 cells were transfected and treated with 2 mM HU for 18 h. WCLs were
1147 prepared, and WB were performed against the indicated proteins, n = 3 independent

1148 experiments. **B.** Western blots from WT RPE1 cells transfected with the indicated
1149 siRNAs and then treated with 1 mM HU for 18 h, n = 3 independent experiments. **C.**
1150 Western blots against the indicated proteins from WT RPE1 cells transfected, then
1151 treated with 1.5 mM HU for 18 h, n = 3 independent experiments. **D.** Comet assay of
1152 hTERT-RPE1 cells treated with 2 mM HU for 40 h. Indicated siRNAs were transfected
1153 two days before HU treatment. Representative comets are shown on the right. Red line
1154 represents median, n = 3 independent experiments, representative experiment shown.
1155 Kruskal-Wallis followed by Dunn's multiple comparison test. ns – not significant. **E.** WT
1156 RPE1 cells were transfected with the indicated siRNAs, then treated with 1.5 mM HU for
1157 18 h and fractioned prior to blotting for the indicated proteins. CE – cytoplasmic extract.
1158 SLX4 values are normalized to H3 loading control, n = 3 independent experiments. **F.**
1159 WT RPE1 cells were transfected and then treated with 2 mM HU for 18 h. Samples
1160 were processed for chromatin fraction prior to blotting for the indicated proteins. RAD51
1161 and SLX4 values are normalized to H3 loading control, n = 3 independent experiments.
1162 **G.** Working model showing proposed roles of BRCA1, RAD51 and SCAI/REV3 upon
1163 fork stalling. See Discussion. Image was partially generated using BioRender.
1164

## SUPPLEMENTARY FIGURE LEGENDS

### Figure S1

**A.** WT RPE1 cells were transfected, then treated with the indicated doses of HU for 18 h and allowed to form colonies. Mean ± SD shown, n = 2 independent experiments. **B.** Representative images from (**A**) are shown. **C.** Immunofluorescence (IF) analyses showing representative RPA foci in WT RPE1 cells post-treatment with indicated siRNAs. Cells were treated with 1 mM HU for 18 h prior to IF. Merge includes RPA foci and DAPI. Scale bars indicate 5 micron. Intensity of nuclear RPA staining was quantified using ImageJ and plotted on the right. ****P < 0.0001 and **P = 0.0063, Ordinary one-way ANOVA followed by Tukey's. **D.** Representative IF images showing γH2AX foci in WT RPE1 cells following treatment with the indicated siRNAs. Cells were treated with 1.5 mM HU for 18 h prior to IF analyses. Scale bars indicate 5 micron. Quantification shown on the right. ****P < 0.0001, ANOVA followed by Tukey's. **E.** Western blots against the indicated proteins from WT RPE1 cells pretreated with 10 μM TLS inhibitor JH-RE-06 or vehicle (DMSO) for 30 min, then treated with 1.5 mM HU for 18 h, n = 3 independent experiments. **F.** WT and SCAI-null U2OS cells were treated with the indicated siRNAs, then treated with 1 mM HU for 18 h prior to blotting for the indicated proteins**,** n = 3 independent experiments.

### Figure S2

**A.** Representative images of 1.5 mM HU-treated RPE1 cells with control or siSCAI at the indicated timepoints showing γH2AX, PCNA, and DAPI staining. Scale bars indicate 50 micron. Note that representative images at the 8 h timepoint is included in the main text with the same images. **B.** Parallel western blot showing SCAI knockdown in RPE1 cells harvested at 8 h after HU. **C.** Quantification of γH2AX intensity from (**A**). T-test, *P < 0.05. Black bars represent mean. **D.** Pearson's correlation coefficient between γH2AX and PCNA measured using BIOP JACoP FIJI plugin using manual thresholding based on control images (γH2AX = 36822; PCNA = 26354). Pearson's correlation was recorded as a single point for each image (n = 14-16) with 10-16 cells per image. Red bars represent mean. **E.** Plot showing the observed overlap between γH2AX and PCNA staining from (**A**), thresholded for both channels at 1.25x10^8 a.u. (dotted line shown in (**C**)). Expected values were obtained by multiplying γH2AX and PCNA positive fractions. **F.** WT RPE1 cells were transfected with the indicated siRNAs and then treated with 2 mM HU for the indicated times. WB were performed against the indicated proteins, n = 3 independent experiments. **G.** Schematic of double thymidine block protocol for cell synchronization. WT RPE1 cells treated with 2 mM thymidine for 16 h, transfected and released for 8 h, treated with 2 mM thymidine for another 16 h, released for 2 h, then harvested for cell cycle analysis by flow cytometry. Representative images shown below. **H.** PLA foci between PCNA and γH2AX on siSCAI 16 h post treatment with 1.5 mM HU. **I.** Quantification of (**H**) with Mean ± SEM for n = 2 independent experiments, with >180 cells/condition/experiment. All experiments were analyzed with One-way ANOVA with a Kruskal-Wallis test for multiple comparisons, *P < 0.0332, **P < 0.0021, ***P < 0.0002, ****P < 0.0001. **J.** Schematic of cell treatment protocol to perform double thymidine block, transfect, and synchronize cells. Comet assay of WT RPE1 cells treated with 2 mM HU for 24 h or untreated. Red line represents median, n = 3

independent experiments, representative experiment shown. Kruskal-Wallis followed by Dunn's multiple comparison test, ****P < 0.0001.

**Figure S3**

**A.** Schematic of pulse-labeling DNA strands. DNA fibers were from RPE1 cells transfected with siRNAs as indicated. New origin firing events (red only) on left panel, percentage of red labels over total number of fibers on the right. Mann-Whitney test, n = 3 independent experiments, ns = not significant. **B.** Schematic of pulse-labeling DNA strands and lengths of two-color DNA fibers. DNA fibers were from hTERT-RPE1 cells transfected with siRNAs as indicated. Red line represents median, n = 2 independent experiments, representative experiment shown. Kruskal-Wallis followed by Dunn's multiple comparison test. *P < 0.05, ****P < 0.0001. **C.** WT RPE1 cells were transfected with the indicated siRNAs, then treated with 1.5 mM HU for 18 h and assayed for the indicated proteins by WB, n = 3 independent experiments.

**Figure S4**

**A.** WT RPE1 cells were transfected with the indicated siRNAs, then treated with 2 mM HU for 18 h before assaying for the indicated proteins by WB, n = 3 independent experiments. **B.** Western blots from WT and SCAI-null U2OS cell lines transfected with the indicated siRNAs and then treated with 1.5 μM cisplatin for 18 h, n = 3 independent experiments. **C.** WT and BRCA1-null RPE1 cells were transfected with the indicated siRNAs, then treated with 1 mM HU for 18 h and fractioned prior to blotting for the indicated proteins. SCAI values are normalized to ORC2 loading control, n = 3 independent experiments. **D.** Comet assay of WT RPE1 following synchronization and siRNA transfection as in **Figure S2J**. Cells treated with 2 mM HU for 24 h. Red line represents median. Kruskal-Wallis followed by Dunn's multiple comparison test. ****P < 0.0001 **E.** Representative images showing cell cycle distribution in WT and BRCA1-null RPE1. Quantified on the right, mean ± SD shown, n = 2 independent experiments.

**Figure S5**

**A.** GFP-WT-BRCA1 rescue (labeled WT), BRCA1-null (Δ), and GFP-BRCA1 Rescued RPE1 cells were assayed for the indicated proteins by WB. **B.** P53-null RPE1 parent (Parent), BRCA1-null (ΔBRCA1), and GFP-WT-BRCA1 Rescue (GFP-BRCA1 Rescue) RPE1 cell lines were transfected and treated with 1 mM HU for 18 h. WCLs were prepared, and WB were performed against the indicated proteins, n = 2 independent experiments.

**Figure S6**

**A.** WT RPE1 cells were transfected with the indicated siRNAs, then treated with 1 mM HU for 18 h and assayed for the indicated proteins by WB, n = 3 independent experiments. **B.** Representative images showing cell cycle distribution in WT RPE1 cells 18 h following treatment with 27 μM B02 compared to vehicle controls. Quantified on the right, mean ± SD shown, n = 2 independent experiments. **C.** Western blots from WT RPE1 cells transfected with the indicated siRNAs, pretreated with DMSO, 10 μM

1255 Olaparib (Olap), or 27 μM B02, and then treated with 1 mM HU for 18h, n = 3
1256 independent experiments.
1257
1258 **Figure S7**
1259 **A.** Parent and BRCA1-null RPE1 cells were transfected and then treated with 3 mM
1260 HU for 18 h. Samples were processed for chromatin fraction prior to blotting for the
1261 indicated proteins, n = 2 independent experiments. **B.** Comet assay of WT RPE1
1262 following synchronization and siRNA transfection as in **Figure S2J**. Cells treated with 2
1263 mM HU for 24 h. Red line represents median. Kruskal-Wallis followed by Dunn's
1264 multiple comparison test. ****P < 0.0001.
1265

# Figure 1

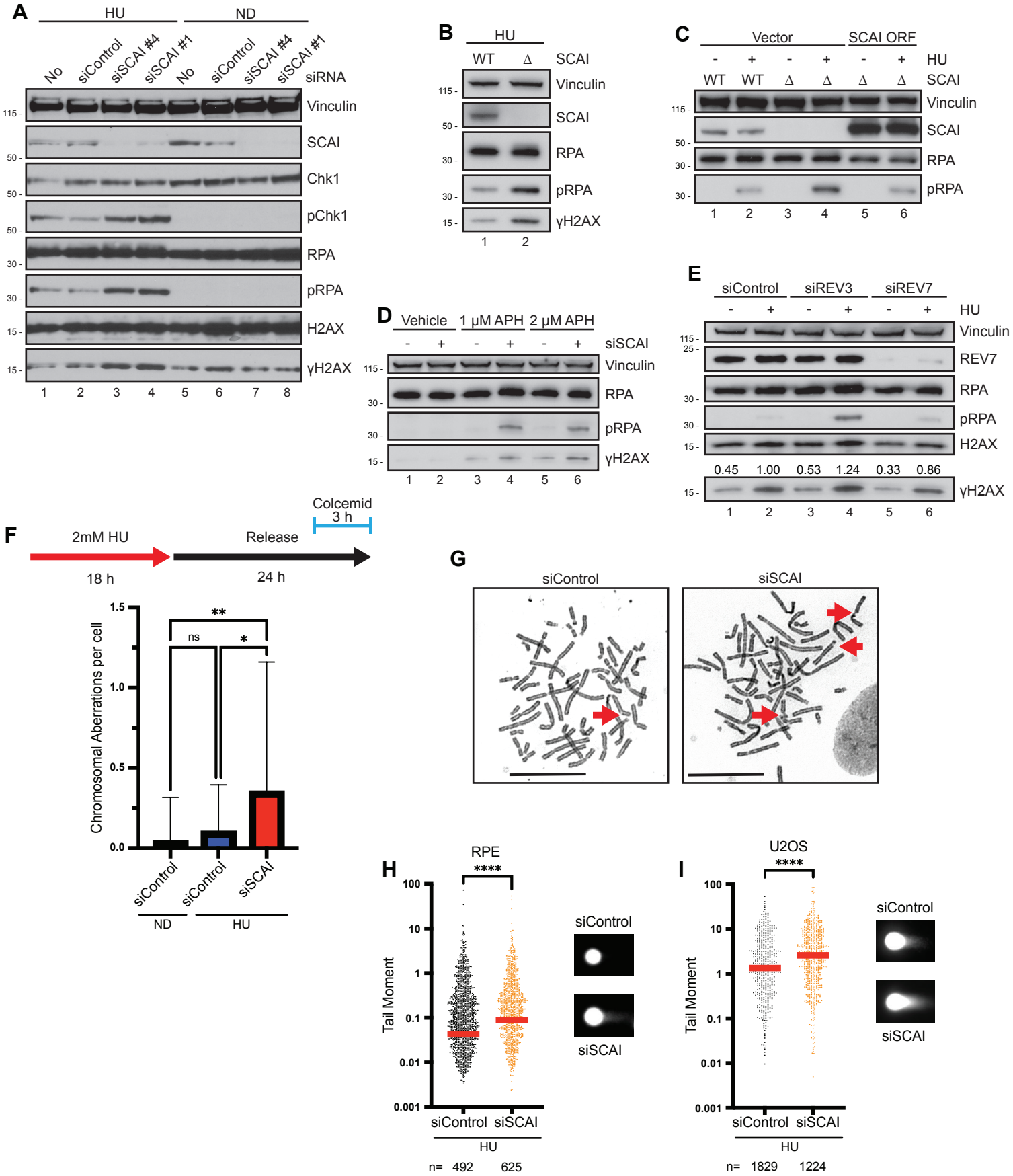
A
HU
ND
No
siControl
siSCAI #4
siSCAI #1
siRNA
Vinculin
SCAI
Chk1
pChk1
RPA
pRPA
H2AX
γH2AX
B
HU
WT
Δ
SCAI
C
Vector
SCAI ORF
HU
D
Vehicle
1 μM APH
2 μM APH
siSCAI
E
siControl
siREV3
siREV7
REV7
0.45
1.00
0.53
1.24
0.33
0.86
F
2mM HU
Release
Colcemid
3 h
18 h
24 h
Chromosomal Aberrations per cell
ns
G
siControl
siSCAI
H
RPE
Tail Moment
n= 492 625
I
U2OS
n= 1829 1224

# Figure 2

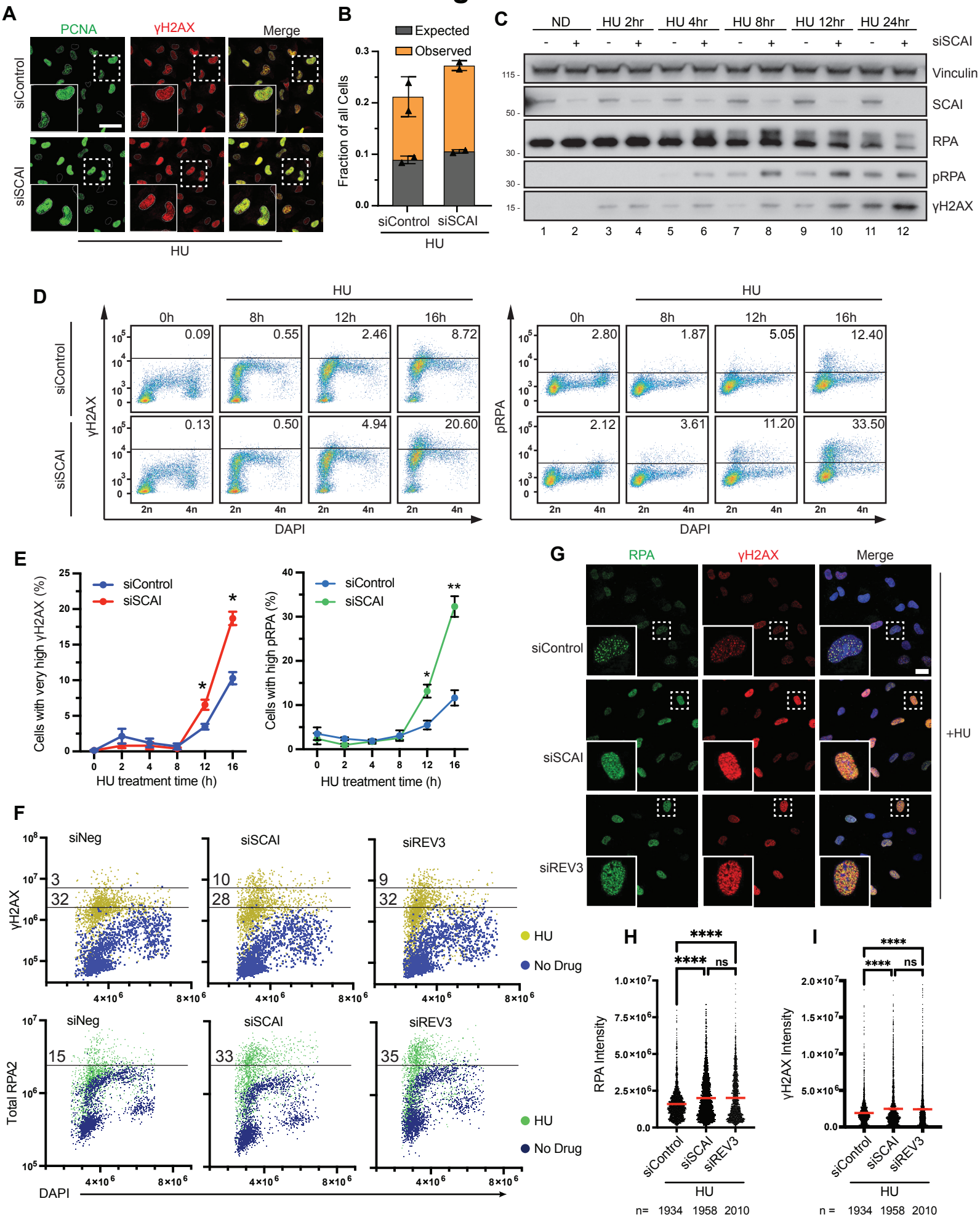
A
PCNA
γH2AX
Merge
siControl
siSCAI
HU
B
Expected
Observed
Fraction of all Cells
siControl
siSCAI
HU
C
ND
HU 2hr
HU 4hr
HU 8hr
HU 12hr
HU 24hr
siSCAI
Vinculin
SCAI
RPA
pRPA
γH2AX
D
HU
0h
8h
12h
16h
siControl
siSCAI
γH2AX
pRPA
DAPI
E
siControl
siSCAI
Cells with very high γH2AX (%)
Cells with high pRPA (%)
HU treatment time (h)
F
siNeg
siSCAI
siREV3
γH2AX
Total RPA2
DAPI
HU
No Drug
G
RPA
γH2AX
Merge
siControl
siSCAI
siREV3
+HU
H
RPA Intensity
siControl
siSCAI
siREV3
HU
n= 1934 1958 2010
I
γH2AX Intensity
siControl
siSCAI
siREV3
HU
n = 1934 1958 2010

# Figure 3

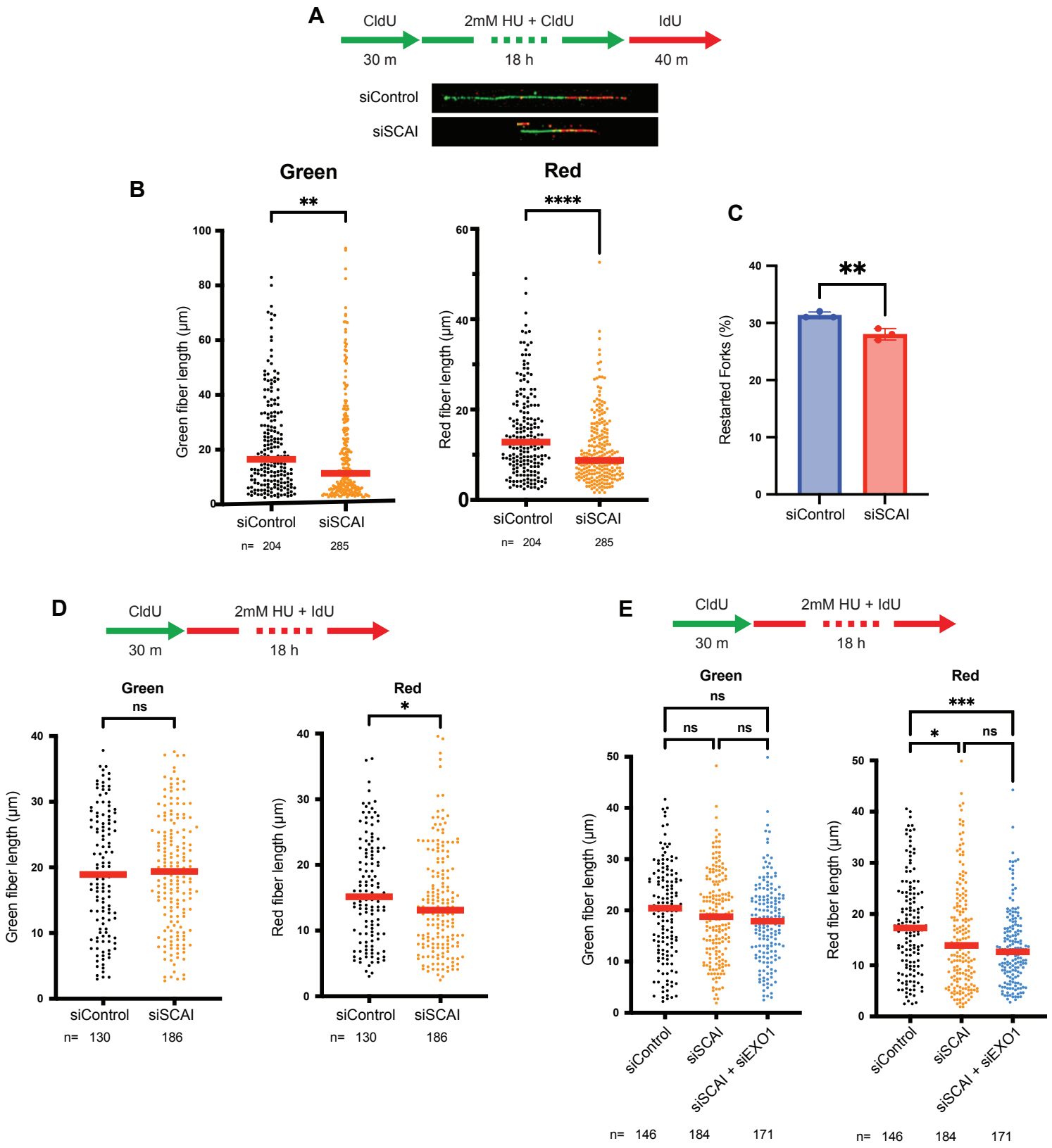
A
CldU
30 m
2mM HU + CldU
18 h
IdU
40 m
siControl
siSCAI
B
Green
Red
**
****
Green fiber length (µm)
Red fiber length (µm)
siControl
siSCAI
n= 204
285
C
**
Restarted Forks (%)
siControl
siSCAI
D
CldU
30 m
2mM HU + IdU
18 h
Green
ns
Red
*
Green fiber length (µm)
Red fiber length (µm)
siControl
siSCAI
n= 130
186
E
CldU
30 m
2mM HU + IdU
18 h
Green
ns
ns
ns
Red
***
*
ns
Green fiber length (µm)
Red fiber length (µm)
siControl
siSCAI
siSCAI + siEXO1
n= 146
184
171

# Figure 4

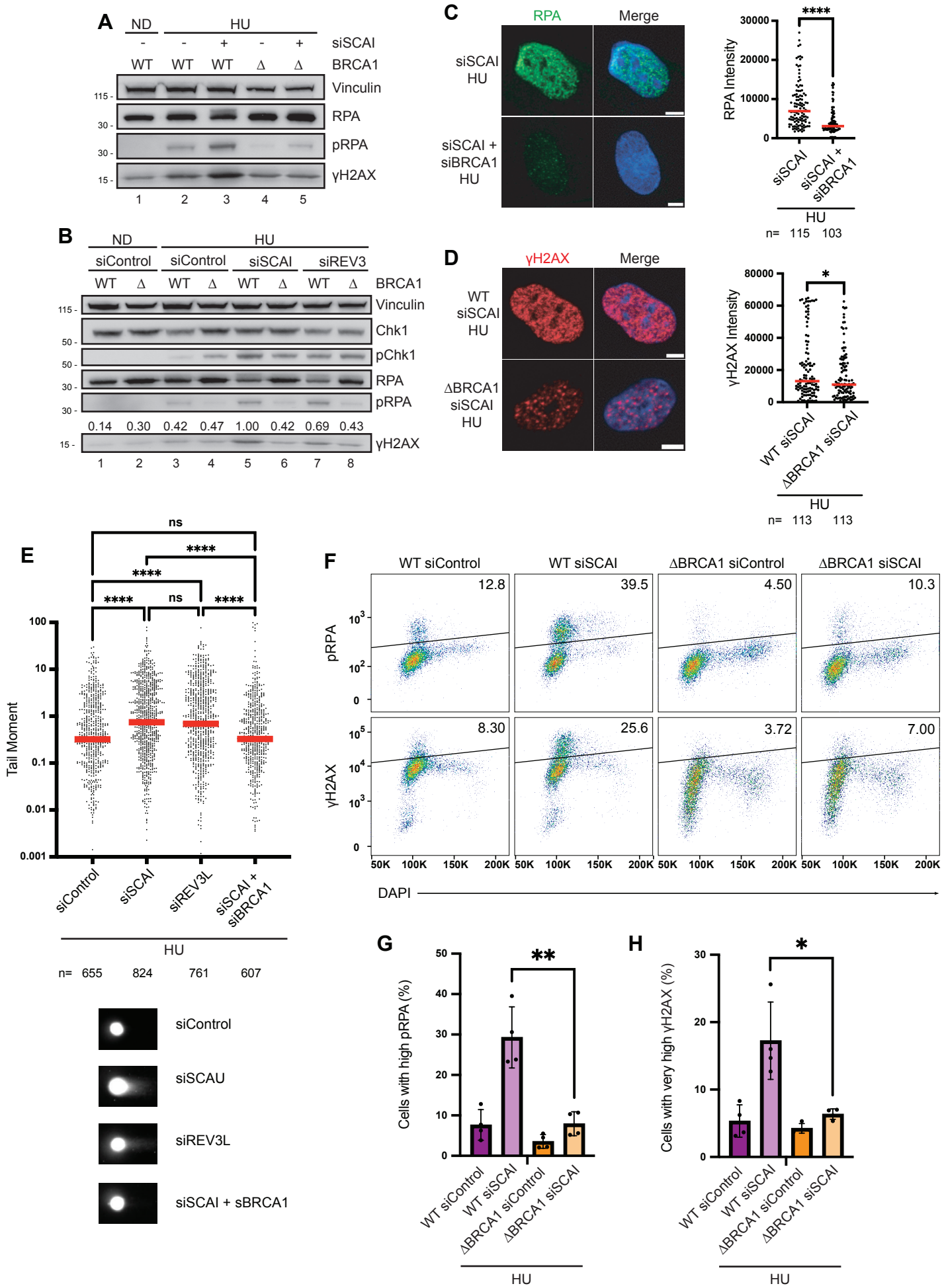
A
ND
HU
siSCAI
BRCA1
WT WT WT Δ Δ
Vinculin
RPA
pRPA
γH2AX
115 -
30 -
30 -
15 -
1 2 3 4 5
B
ND
HU
siControl
siControl
siSCAI
siREV3
WT Δ WT Δ WT Δ WT Δ
BRCA1
Vinculin
Chk1
pChk1
RPA
pRPA
γH2AX
115 -
50 -
50 -
30 -
30 -
15 -
0.14 0.30 0.42 0.47 1.00 0.42 0.69 0.43
1 2 3 4 5 6 7 8
C
RPA
Merge
siSCAI HU
siSCAI + siBRCA1 HU
RPA Intensity
30000
20000
10000
0
****
siSCAI
siSCAI + siBRCA1
HU
n= 115 103
D
γH2AX
Merge
WT siSCAI HU
ΔBRCA1 siSCAI HU
γH2AX Intensity
80000
60000
40000
20000
0
*
WT siSCAI
ΔBRCA1 siSCAI
HU
n= 113 113
E
ns
****
****
****
ns
****
Tail Moment
100
10
1
0.1
0.01
0.001
siControl
siSCAI
siREV3L
siSCAI + siBRCA1
HU
n= 655 824 761 607
siControl
siSCAU
siREV3L
siSCAI + sBRCA1
F
WT siControl
WT siSCAI
ΔBRCA1 siControl
ΔBRCA1 siSCAI
12.8
39.5
4.50
10.3
8.30
25.6
3.72
7.00
pRPA
γH2AX
50K 100K 150K 200K
DAPI
G
Cells with high pRPA (%)
50
40
30
20
10
0
**
WT siControl
WT siSCAI
ΔBRCA1 siControl
ΔBRCA1 siSCAI
HU
H
Cells with very high γH2AX (%)
30
20
10
0
*
WT siControl
WT siSCAI
ΔBRCA1 siControl
ΔBRCA1 siSCAI
HU

# Figure 5

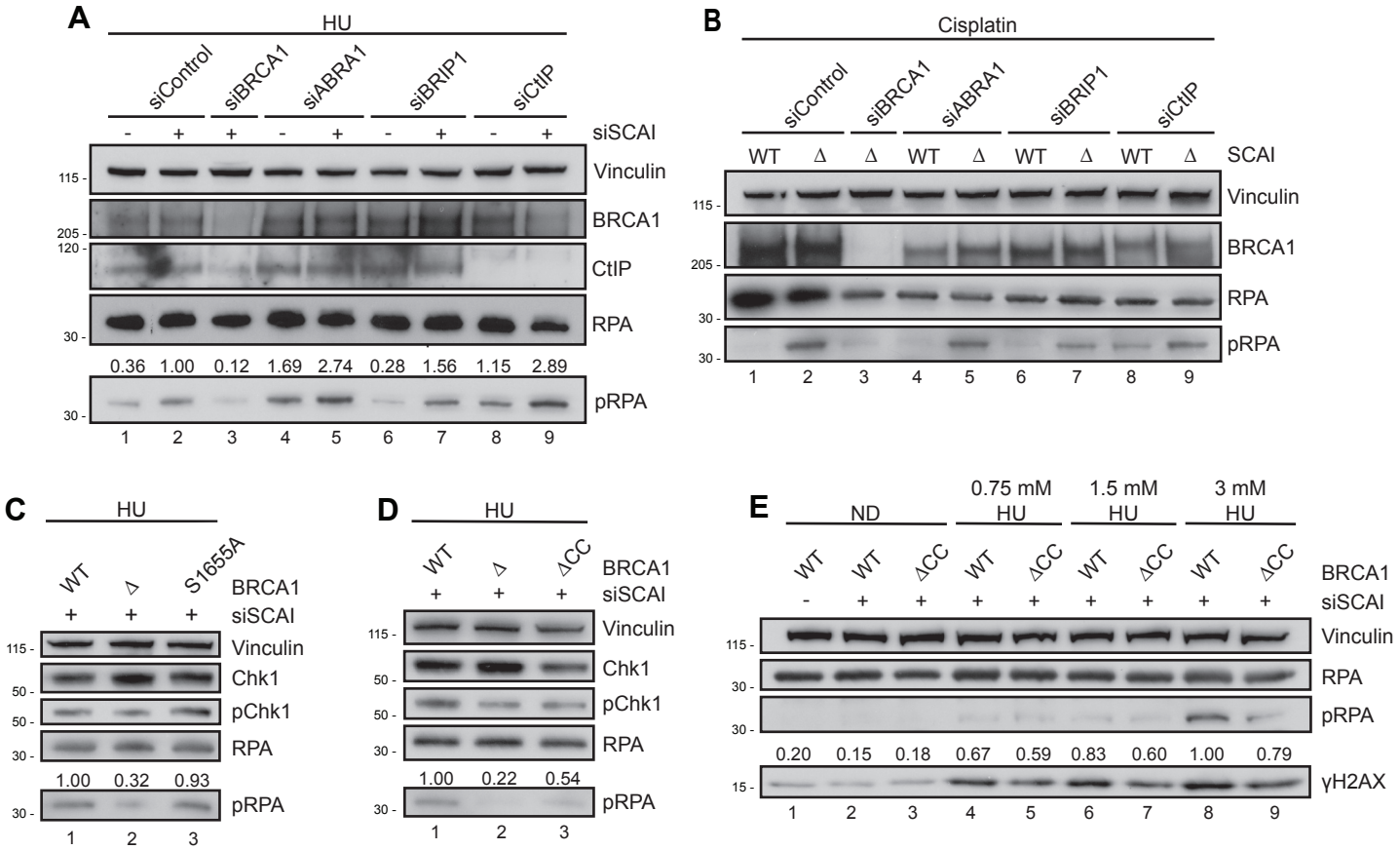
A
HU
siControl
siBRCA1
siABRA1
siBRIP1
siCtIP
siSCAI
Vinculin
BRCA1
CtIP
RPA
pRPA
115 -
205 -
120 -
30 -
0.36 1.00 0.12 1.69 2.74 0.28 1.56 1.15 2.89
1 2 3 4 5 6 7 8 9
B
Cisplatin
siControl
siBRCA1
siABRA1
siBRIP1
siCtIP
WT Δ Δ WT Δ WT Δ WT Δ
SCAI
Vinculin
BRCA1
RPA
pRPA
115 -
205 -
30 -
1 2 3 4 5 6 7 8 9
C
HU
WT
Δ
S1655A
BRCA1
siSCAI
Vinculin
Chk1
pChk1
RPA
pRPA
115 -
50 -
30 -
1.00 0.32 0.93
1 2 3
D
HU
WT
Δ
ΔCC
BRCA1
siSCAI
Vinculin
Chk1
pChk1
RPA
pRPA
115 -
50 -
30 -
1.00 0.22 0.54
1 2 3
E
ND
0.75 mM HU
1.5 mM HU
3 mM HU
WT WT ΔCC WT ΔCC WT ΔCC WT ΔCC
BRCA1
siSCAI
Vinculin
RPA
pRPA
γH2AX
115 -
30 -
15 -
0.20 0.15 0.18 0.67 0.59 0.83 0.60 1.00 0.79
1 2 3 4 5 6 7 8 9

# Figure 6

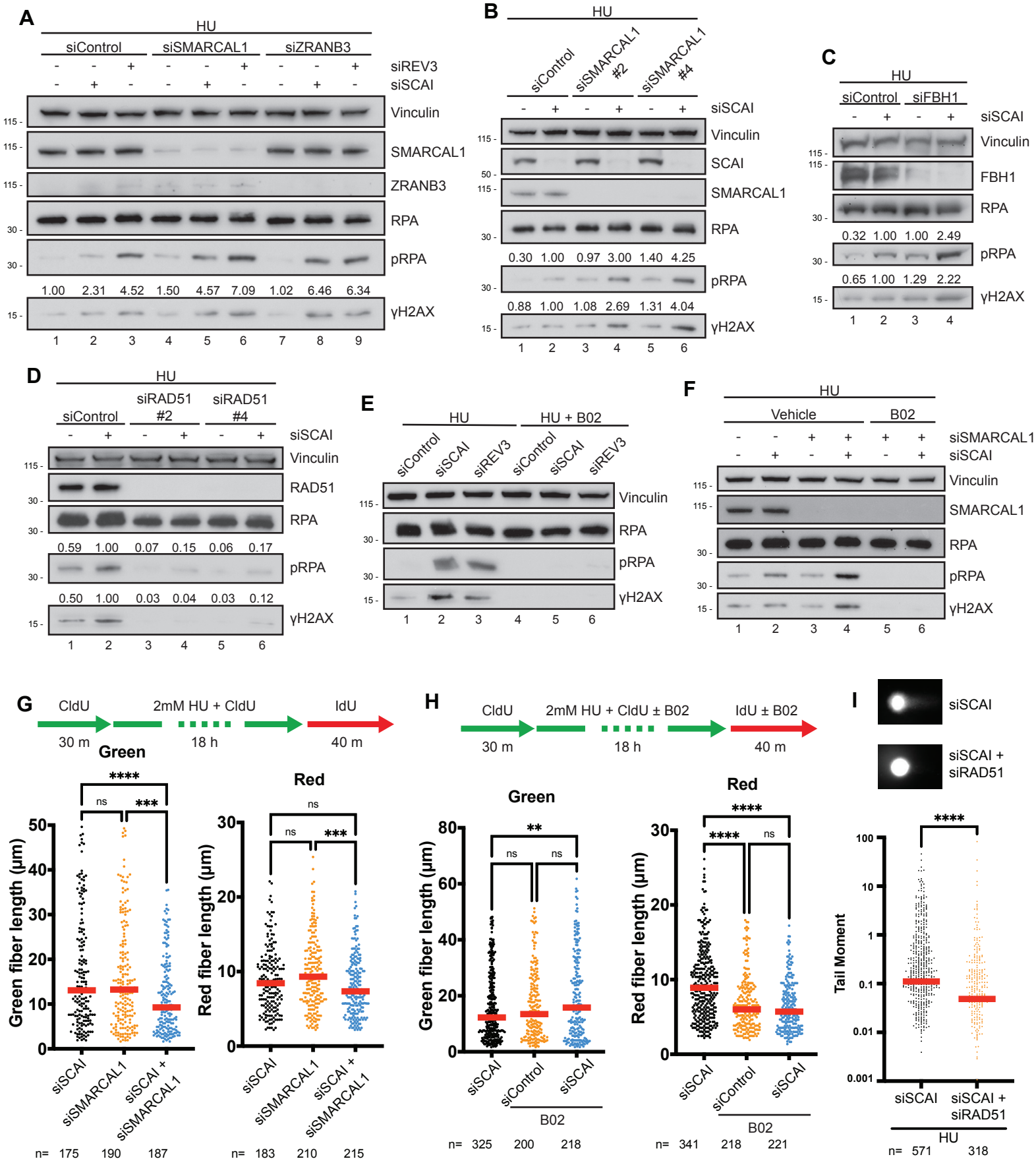
A
HU
siControl
siSMARCAL1
siZRANB3
siREV3
siSCAI
Vinculin
SMARCAL1
ZRANB3
RPA
pRPA
γH2AX
1.00 2.31 4.52 1.50 4.57 7.09 1.02 6.46 6.34
B
HU
siControl
siSMARCAL1 #2
siSMARCAL1 #4
siSCAI
Vinculin
SCAI
SMARCAL1
RPA
pRPA
γH2AX
0.30 1.00 0.97 3.00 1.40 4.25
0.88 1.00 1.08 2.69 1.31 4.04
C
HU
siControl
siFBH1
siSCAI
Vinculin
FBH1
RPA
pRPA
γH2AX
0.32 1.00 1.00 2.49
0.65 1.00 1.29 2.22
D
HU
siControl
siRAD51 #2
siRAD51 #4
siSCAI
Vinculin
RAD51
RPA
pRPA
γH2AX
0.59 1.00 0.07 0.15 0.06 0.17
0.50 1.00 0.03 0.04 0.03 0.12
E
HU
HU + B02
siControl
siSCAI
siREV3
Vinculin
RPA
pRPA
γH2AX
F
HU
Vehicle
B02
siSMARCAL1
siSCAI
Vinculin
SMARCAL1
RPA
pRPA
γH2AX
G
CldU
2mM HU + CldU
IdU
30 m
18 h
40 m
Green
Red
Green fiber length (µm)
Red fiber length (µm)
****
***
ns
siSCAI
siSMARCAL1
siSCAI + siSMARCAL1
n= 175 190 187
n= 183 210 215
H
CldU
2mM HU + CldU ± B02
IdU ± B02
30 m
18 h
40 m
Green
Red
Green fiber length (µm)
Red fiber length (µm)
**
****
ns
siSCAI
siControl
B02
n= 325 200 218
n= 341 218 221
I
siSCAI
siSCAI + siRAD51
Tail Moment
****
HU
n= 571 318

# Figure 7

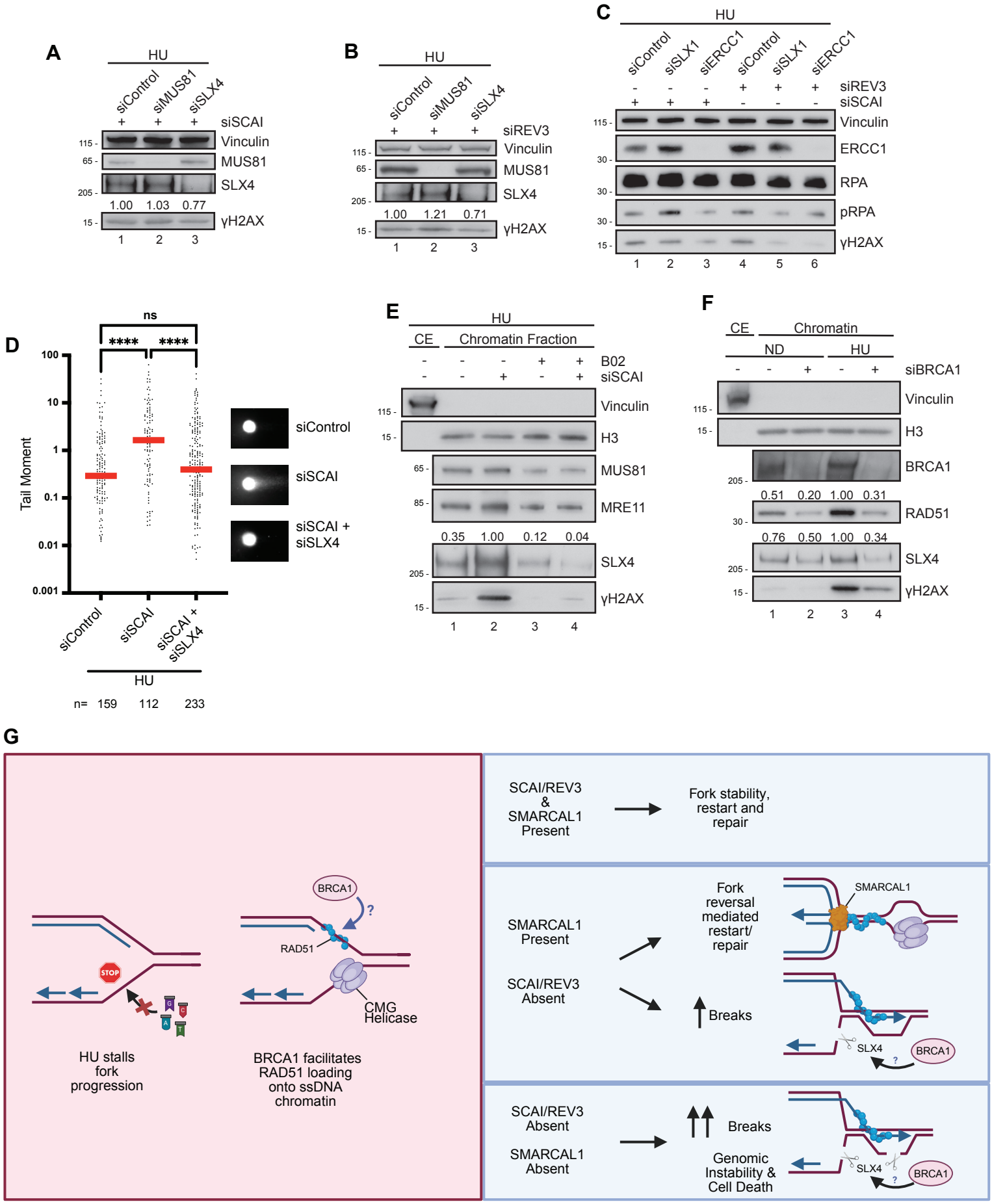
A
HU
siControl
siMUS81
siSLX4
siSCAI
Vinculin
MUS81
SLX4
1.00 1.03 0.77
γH2AX
B
HU
siControl
siMUS81
siSLX4
siREV3
Vinculin
MUS81
SLX4
1.00 1.21 0.71
γH2AX
C
HU
siControl
siSLX1
siERCC1
siREV3
siSCAI
Vinculin
ERCC1
RPA
pRPA
γH2AX
D
ns
****
****
Tail Moment
siControl
siSCAI
siSCAI + siSLX4
HU
n= 159 112 233
E
HU
CE
Chromatin Fraction
B02
siSCAI
Vinculin
H3
MUS81
MRE11
0.35 1.00 0.12 0.04
SLX4
γH2AX
F
CE
Chromatin
ND
HU
siBRCA1
Vinculin
H3
BRCA1
0.51 0.20 1.00 0.31
RAD51
0.76 0.50 1.00 0.34
SLX4
γH2AX
G
STOP
HU stalls fork progression
BRCA1
RAD51
CMG Helicase
BRCA1 facilitates RAD51 loading onto ssDNA chromatin
SCAI/REV3 & SMARCAL1 Present
Fork stability, restart and repair
SMARCAL1 Present
Fork reversal mediated restart/ repair
SMARCAL1
SCAI/REV3 Absent
Breaks
SLX4
BRCA1
SCAI/REV3 Absent
SMARCAL1 Absent
Breaks
Genomic Instability & Cell Death
SLX4
BRCA1